Modeling electric vehicle charging station expansion with an integration of renewable energy and Vehicle-to-Grid sources

Md Abdul Quddus*, Mohannad Kabli, Mohammad Marufuzzaman

Department of Industrial and Systems Engineering, Mississippi State University, Starkville, MS 39759-9542, United States

ABSTRACT

This study proposes a novel formulation for designing and managing electric vehicle charging stations, considering both long-term planning decisions and short-term operational decisions over a pre-specified planning horizon and under stochastic power demand. To solve this challenging problem, we propose a hybrid algorithm that combines Sample Average Approximation with an enhanced Progressive Hedging Algorithm. A case study, based on the road network around Washington, D.C., is presented to visualize and validate the modeling results. Results indicate that the electric vehicle power demand are satisfied primarily via the grid and Vehicle-to-Grid when energy cost is low and solar power is unavailable.

1. Introduction

Fossil fuel has been the dominant energy source for transportation vehicles over a long period of time. The technology in cars has advanced significantly in every aspect except energy sources they are running. Several attempts were made to replace fossil fuels with other forms of energy such as natural gas, electricity, hydrogen, and hybrid fuels. Fossil fuels are limited and will have to be replaced by other energy sources. Advancing of the technology of renewable energy serves to that effect. Another advantage of using renewable resources is the lower in Greenhouse Gas (GHG) emissions which is gained by using less energy from fossil fuels and more from natural resources. Attempts to replace fossil fuels were few and inefficient. Furthermore, *range anxiety*[1] is one of the major reasons for slowing down the adoption rate of electric vehicles (Nilsson, 2011). Fortunately, a number of recent advancements in battery technology, along with the continuation of research in this area, are striving to alleviate this problem in future. For instance, a recent advancement in lithium-ion batteries let Tesla run their electric vehicles over 300 miles.[2] Samsung, on the other hand, developed a lithium-ion battery that can be fully charged in 20 min and makes electric vehicles to go over 370 miles.[3] Another barrier for promoting electric vehicles is the lack of charging stations which, if constructed carefully over time, would improve the use of electric vehicles in the future (Kuby and Lim, 2005). Finally, a number of initiatives from the U.S. government, such as *Electric Vehicle Everywhere Grand Challenge*, will support the growth of electric vehicles in coming years (U.S. Department of Energy, 2014). The collaboration in the investment strategies between the light duty electric vehicles (LDEV) and electricity generation sectors can substantially reduce the total societal cost (i.e., the sum of costs from both sectors) (Chen et al., 2017). To cope with this projected

---

* Corresponding author.
E-mail addresses: mq90@msstate.edu (M.A. Quddus), mrk297@msstate.edu (M. Kabli), maruf@ise.msstate.edu (M. Marufuzzaman).

[1] Range anxiety refers to continual concern and fear of the electric vehicle's occupants of becoming stranded with a discharged battery before reaching destination.
[2] Available from: https://www.tesla.com/charging.
[3] Available from: https://electrek.co/2017/01/09/samsung-2170-battery-cell-tesla-panasonic/.

growth, there is a need to carefully design and manage electric vehicle charging stations to not only reduce the overall system costs but also to provide substantial environmental and social benefits for the community. As the penetration of electric vehicle spreads, the load on the power system is going to increase due to the expansion of the charging infrastructure. A recent study from the Washington State's Department of Transportation reveals that a total of 228,725 kWh of energy was supplied to charge electric cars between 2012 and 2015, which is equivalent to replacing 22,397 gallons of gas (Washington State Department of Transportation, 2015). Further, projections are made that the load from electric vehicles in the state of Washington will reach around 107 MW by 2029 (City Light, 2010). Bai et al. (2015) demonstrate the effect of the daily load curve triggered by an electric vehicle considering three different modes of charging. The authors have found that electric vehicles have significant impact on the daily load curve. To hedge against this projected growth, it may be required to upgrade electricity distribution systems, increase capacities, integrate renewable energy sources (RES), introduce dynamic pricing options (i.e., encourage off-peak charging so that the growing loads do not exacerbate peak demand), and many more.

Charging stations heavily rely on electric power systems. Since the electricity demand and supply must be equal at all times, generation, transmission, and distribution capacities need to be designed accordingly to cope with any anticipated peak demand. This can be better achieved by integrating *renewable* sources withthe *Vehicle-to-Grid* (V2G) services, where cars will have the option to sell back the excess energy in their vehicle's batteries to the grid. The V2G allows car batteries to act as a portable storage for energy. The RES, also known as *green energy*, are generated using natural resources, such as solar rays, wind, or river streams, and are subject to varying degrees of uncertainty. For instance, solar and wind energies depend on the availability of sun, weather fronts, and other complex phenomena. On the other hand, V2G services allow charging stations to discharge electricity back to the grid when connected and thus lead to greater renewable-integration benefits. In the V2G mode, electric vehicles can discontinue charging and start discharging their batteries in exchange for some incentive, if the charging stations experience any sudden increase in demand or unexpected interruption from renewable sources. It is worth noting that, though the benefits of using these sources are obvious, challenges lie on predicting their availabilies in hours ahead. Renewable energy variability and uncertainty cause a number of power system operational and planning challenges for the power companies since real-time electricity supply and demand must be in exact balance at all times to maintain power system stability and reliability (Weiller and Sioshansi, 2016). Furthermore, since the sources of V2G energy are heavily reliant on electric vehicles passing through the charging stations and highly stochastic in nature, therefore, the availability of V2G services vary significantly in different time periods of the day. Therefore, even though the benefits of integrating renewable energy with V2G are already realized, charging stations still find difficulty to optimize their operations to receive the true benefits from this integration.

Up until now, a stream of research has addressed the charging scheduling problem. Of those, many have considered the integration of renewable energy with or without V2G sources while planning charging schedules for the electric vehicles. Liu et al. (2012) study how the smart charging patterns of electric vehicles affect the power system scheduling while considering coordination of wind energy, thermal units, and V2G sources. He et al. (2012) present a global and a local scheduling model to decide on charging and discharging decisions for the electric vehicles with an aim of minimizing the overall system cost. Ortega-Vazquez et al. (2013) study how the integration of V2G with power systems can be made to achieve better efficiency and security. Results show that this coordination will allow to operate efficiently under the existing power infrastructure. Haddadian et al. (2016) study the effects of considering V2G and renewable energy as viable sources for the smart grid. The impact of electric vehicles as mobile sources of energy is studied to hedge against the peak load hours and make the power supply more stable. Jin et al. (2014) propose a stochastic optimization model to minimize the average cost of using renewable energy under its supply uncertainty. Hong et al. (2015) plan for the operations of charging stations by considering different pricings throughout the day while integrating renewable energy into the power system.

Another stream of research is dedicated to the applications of battery swap stations where the electric vehicles can exchange their depleted or nearly depleted batteries with full batteries for a fee. Pan et al. (2010) present a two-stage stochastic programming model that determines where to locate battery swap stations and then make appropriate operational decisions (*e. g.*, number of batteries to charge and discharge) based upon realized battery demands, electric vehicle loads, and production of renewable energies. A salient feature of the model is that it allows for battery discharge to support grid during peak hours. Worley and Klabjan (2011) present a dynamic programming model that determines the number of batteries to purchase and their charging time based on dynamic changes in grid power fees. Mak et al. (2013) develop two robust optimization models where one minimizes costs while the other one maximizes a pre-specified amount of profit associated with optimizing the infrastructure planning for battery swap stations. Nurre et al. (2014) develop a mathematical model to determine the optimal operational decisions (e.g., number of batteries to charge, discharge, and exchange) of a battery swap station over a pre-specified time horizon. Liu et al. (2014) propose an optimization model to determine the energy exchange strategies of a battery swap station by considering solar energy availability. Along the same line, Liu et al. (2016) extend the previous study to determine the location and capacity of battery swap stations while considering the energy demand management decisions (*e. g.*, optimal pricing, number of batteries to charge and discharge).

Realizing the need that the energy demand may fluctuate highly from one hour to the next, imposes most of the studies discussed above which attempt to manage charging station decisions on an hourly basis. However, the studies fail to provide an expansion plan for the charging stations. The principal challenge that must be overcome in order to replace petroleum powered passenger vehicles with electric vehicles is to concurrently locate and manage charging station decisions efficiently over a specified planning horizon. This is practical since potential consumers will be less inclined to purchase electric vehicles unless there is an adequate charging station infrastructure (Bento, 2008). In pursuit of this goal, a new stream of research has attempted to extend the single time period flow-refueling location model (FRLM), introduced by Kuby and Lim (2005). Of those, we mention the works done by Hosseini and MirHassani (2015) and Li et al. (2016). Recently, Vries and Duijzer (2017) prove FRLM as strongly NP-hard, and propose a mixed-

integer linear programming formulation for the FRLM. The authors also extend to the case for which the driving range varies during a trip. Others have tackled the same problem using different perspectives. For example, Sweda and Klabjan (2011) identify the patterns in residential electric vehicle ownership and driving activities by developing an agent-based decision support system to allow strategic deployment of new charging stations. Ge et al. (2011) optimize the sizing and siting of electric vehicle charging stations and minimize the cost of charging stations. A mathematical program model is presented and solved using an active-set decomposition algorithm. Ip et al. (2010) use a clustering technique that compile data points, containing quantified road information of electric vehicle charging demand in an urban setting, to inform the location plans for the electric vehicle charging stations. Bhatti et al. (2015) study a two-stage optimal location decision problem, where the demand information is learned over time. A key feature of the model is to provide a solution for whether to actively learn the market through a greater initial investment in the alternative fuel stations network or to deter the commitment since an overly aggressive investment often results in sub-optimal alternative fuel station locations.

To the best of the authors' knowledge, no prior studies have integrated both the long-term charging station planning decisions (*e. g*., size, location, and time to open charging stations) and short-term hourly operational decisions (*e. g*., number of batteries charged, discharged through B2G, stored, V2G, renewable, grid power usage) under the same decision making framework. To fill this gap in the literature, this study proposes a two-stage stochastic programming model that simultaneously optimizes long-term planning decisions and short-term charging station management decisions over a pre-specified planning horizon and under stochastic power demand. The problem is challenging due to the $\mathcal{NP}$-hard nature of location design, uncertainties present in dynamic traffic demands, availability in RES, and many others which significantly impact the hourly power management (*e. g*., renewable, V2G, grid power usage) and battery charging, discharging, and storage decisions in a charging station. To alleviate these modeling challenges and to solve real scale problem instances, we propose a customized hybrid algorithm that combines Sample Average Approximation (SAA) with an enhanced Progressive Hedging Algorithm (PHA). The hybrid algorithm incorporates several algorithmic improvements such as penalty parameter updating techniques, local and global heuristics, and different variants of the rolling horizon heuristic. We apply this algorithm to solve a real world case problem by using the road network of Washington, D.C. and to cast a number of managerial insights into the optimal system design and the total system cost. Table 1 distinguishes our contribution with the existing electric vehicle literatures. In summary, the main contributions of this paper to the existing literature are as follows:

1. We develop a two-stage stochastic mixed-integer program that incorporates both long term planning decisions and short-term hourly operational decisions to design and manage electric vehicle charging station decisions under stochastic power demand. The proposed model differs from existing studies in that:
   (a) We consider a long-term charging station expansion planning model that features size, location, and timing to open facilities and demand response with a short-term hourly time resolution. We notice from the existing body of literature that there are models that capture either long-term charging station planning decisions or short-term operational charging stations managing decisions. However, none of the prior studies have investigated the integrated effects for both long-term charging station planning and short-term hourly operational decisions under the same decision making framework. Separate considerations of these models, as observed in prior studies, may result in sub-optimal decisions or inaccurate cost estimation. The integration of these considerations is motivated by real cases and indeed poses methodological challenges. Upon solving efficiently, this holistic approach holds promise to enhance engineering guidelines and policies which are crucial for the sustainment of this new vehicular system.
   (b) We extend the model by introducing chance and expected value constraints to ensure high renewable energy utilization. Experimental results indicate that this integration has profound impact on minimizing the overall system cost.
2. We develop and implement a customized hybrid solution approach that combines a Sample Average Approximation algorithm with an enhanced Progressive Hedging Algorithm to solve our proposed optimization model. We introduce a number of algorithmic improvements such as penalty parameter updating techniques, local and global heuristics, and different variants of the rolling horizon heuristic.
3. We construct a real-world case study to test the performance of the algorithms and to reveal interesting managerial insights. We demonstrate the computational performance of our customized hybrid algorithm relative to its generic version. As evidenced from a set of computational results that the enhanced variant of the hybrid algorithm is capable of producing high-quality solutions consistently to solve realistic large-size problem instances by obeying the termination criteria.

The exposition of this paper is as follows. Section 2 introduces a two-stage stochastic programming model for designing and managing long-term and short-term electric vehicle charging station decisions under power demand uncertainty. The hybrid solution approach to solve our proposed optimization model is introduced in Section 3. Section 4 performs a series of computational experiments to draw managerial insights and to verify the performance of the algorithms. Section 5 concludes this paper and provides some future research directions.

2. Problem description and model formulation

This section discusses the electricity flow of the transportation network. The problem description is provided which is followed by a two-stage stochastic mixed-integer linear programming (MILP) model to solve the research problem optimally. The key purpose is to minimize the overall energy network cost of electricity flow with respect to established charging stations, which allows decision makers to serve electricity demands in an efficient way.

Table 1
Distinguishing our study with related electric vehicle literature.

References	Problem Types	Modeling Techniques	Solution Methods	Time Period	Energy Sources	Station Types
Ge et al. (2011)	D[1]	LP[3]	N/A	Single	Grid	CS[12]
Wang et al. (2010)	D	NLP[4]	Demand Priority Heuristics	Single	Grid	CS
He et al. (2012)	D	NLP	N/A	Single	Grid & V2G	CS
Ortega-Vazquez et al. (2013)	D	MILP	N/A	MH[9]	Grid, V2G, & Renewable	CS
Liu et al. (2014)	D	NLP	GA[6]	MH	Grid & Renewable	BSS[13]
Nurre et al. (2014)	D	Integer Program	N/A	MH	Grid, V2G, & Renewable	BSS
Fathabadi (2015)	D	LP	N/A	Single	Grid, V2G, & Renewable	CS
Pan et al. (2010)	S[2]	Two-stage stochastic MILP	N/A	Single	Grid, V2G, & Renewable	BSS
Worley and Klabjan (2011)	S	Dynamic Programming	PLA[7]	MH	Grid	BSS
Mak et al. (2013)	S	MISCP[5]	N/A	Single	Grid	BSS
Hong et al. (2015)	S	Probabilistic Model	GA	MH	Grid & Renewable	CS
Jin et al. (2014)	S	Stochastic Optimization	Lyapunov Optimization	MH	Grid & Renewable	CS
Liu et al. (2012)	S	Two-stage stochastic MILP	N/A	MH	Grid, V2G, & Renewable	CS
Shojaabadi et al. (2016)	S	LP	MCS[8] & GA	MY[10]	Grid & V2G	CS
Haddadian et al. (2016)	S	MILP	Benders Decomposition	MH	Grid, V2G, & Renewable	CS
Kavousi-Fard and Khodaei (2016)	S	Constrained Optimization	N/A	MH	Microgrid	CS
Our study	S	Two-stage stochastic MILP	Hybrid algorithm combines SAA with PHA	MHY[11]	Grid, V2G, & Renewable	CS & BSS

[1] D: Deterministic.

[2] S: Stochastic.

[3] LP: Linear Program.

[4] NLP: Non-linear Programming.

[5] MISCP: Mixed-integer Second-order Cone Program.

[6] Genetic Algorithm.

[7] PLA: Piecewise Linear Approximation.

[8] MCS: Monte Carlo Simulation.

[9] MH: Multi-hour.

[10] MY: Multi-year.

[11] MHY: Multi-(hour & year).

[12] CS: Charging Station.

[13] BSS: Battery Swapping Station.
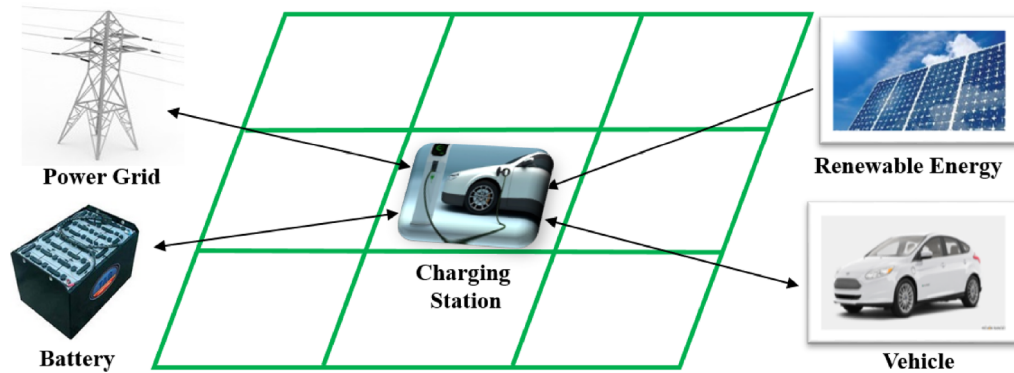
Fig. 1. Network illustration of integration of different energy sources with a charging station.

2.1. Problem description

We develop a two-stage stochastic MILP model that simultaneously addresses long-term electric vehicle charging station expansion decisions (*e. g.*, facility location decisions) and short-term hourly operational decisions (*e. g.*, number of batteries charged, discharged through B2G, stored, V2G, renewable, grid power usage) over a pre-specified planning horizon and under power demand uncertainty. To serve this purpose, the transportation network is divided into a set of cells $\mathcal{I}$, where each cell can be considered as a potential location to establish a charging station over a set of time periods, including a set of hours $\mathcal{H}$ and a set of years $\mathcal{T}$.

A two-way connection between the power grid (PG) and electric vehicle (EV) charging station is used, allowing the station to buy electricity from the grid when needed and sell back to the grid through Battery-to-Grid (B2G) when it is profitable. In this research, two types of charging stations are considered with respect to their electric supply capacities. A *type 1* charging station includes the PG, the RES, and the V2G usage as power sources, while a *type 2* charging station includes swappable batteries in addition to the power sources available for *type 1* charging stations. After opening a charging station, we assume that the electricity demand in the charging station can be supplied from four different energy sources: (*i*)PG; (*ii*) stored batteries at the charging stations; (*iii*)RES (e.g., solar power); and (*iv*) discharged power of electric vehicles into the grid through the V2G connection capabilities. Fig. 1 shows how different energy sources are integrated with a charging station in a transportation network.

It is worth noting that long-term decisions, which require large budgets, are sometimes desired to be provided in advance for the entire predefined planning horizon. The charging station opening decision is a key strategic long-term decision which provides the necessary infrastructure to accommodate electric vehicle charging needs and participate in increasing the ownership base of electric vehicles. Hence, we assume that the number of time-stages are predetermined and each time-stage has an equal length (for both hours and years). Moreover, short-term operational decisions are made on an hourly basis and we use a representative 24 h period from each year of the planning horizon as the short-term operational decisions. Even though the operations of a charging station occur continuously over time, we divide a day into 24 h to ease traceability. The representative 24 h demand is equivalent to the average demand of the whole year. We further assume the charging station opening decisions are made at the beginning of each year.

Estimating electric vehicles' flow is a challenging problem, and it can be even more difficult depending upon traffic and road geometry (*e. g.*, curvy links). A rough estimation of flow is obtained by: (*i*) developing a routing algorithm that deploys electric vehicles from multiple sources to destination points to get an estimation of the number of vehicles passed through each link of the real world physical network, and then (*ii*) developing cells on the network obtained from (*i*) to estimate the number of electric vehicles passing through each cell in a given time period. Additionally, electric vehicles' flow also fluctuates highly from one hour to another. This mandates the necessity to investigate a large scenario set for electric vehicles' flow in developing a two-stage stochastic programming model. While doing so, we consider the available electric vehicles in our tested region into account that helps in predicting the future availability of electric vehicles. Then, we use the Monte Carlo simulation to generate scenarios for electric vehicles' flow in our tested regions. The demand of each cell is modeled as an uncertain variable of which probability distribution might not be known in advance. Electricity demand of each cell is determined in terms of the expected number of electric vehicles traversed through the cell in each time period and, consequently, the percentage of those that requires to be charged under each scenario. Similarly, expected V2G electricity availability is determined in terms of the percentage of electric vehicles required to be discharged in each time period and under each scenario. It is worth noting that this way we have indirectly considered the drivers' behavior in charging station choice.

2.2. Model formulation

Let us now summarize the following notation for our two-stage stochastic programming model. Parameters are introduced by lowercase and Greek letters, while variables are introduced by uppercase letters. Additionally, the superscripts of parameters represent their brief descriptions while their subscripts represent their indices.

Sets:

- $\mathcal{I}$: set of cells
- $\mathcal{T}$: set of years
- $\mathcal{H}$: set of hours
- $\mathcal{K}$: set of station types (K_1 to denote *type 1* charging stations and K_2 to denote *type 2* charging stations with battery swap stations, *i.e.*, $\mathcal{K} = \{K_1, K_2\}$)
- Ω: set of scenarios

Parameters:

- ψ_{ikt}: annualized cost of constructing and maintaining a charging station of type $k \in \mathcal{K}$ at cell $i \in \mathcal{I}$ in year $t \in \mathcal{T}$
- f_{iht}: flow of electric cars at cell $i \in \mathcal{I}$ in hour $h \in \mathcal{H}$ of year $t \in \mathcal{T}$
- λ: average unit power requirement for each car (in kWh)
- γ: average unit power discharged from each car (in kWh)
- $\eta_{ht\omega}$: percentage of the car charged on hour $h \in \mathcal{H}$ of year $t \in \mathcal{T}$ under scenario $\omega \in \Omega$
- β_{ht}: percentage of the car discharged power on hour $h \in \mathcal{H}$ in year $t \in \mathcal{T}$
- c_{ht}^{pg}: unit PG electricity cost consumed by EV in hour $h \in \mathcal{H}$ of year $t \in \mathcal{T}$ ($\$$/kWh)
- c_{ht}^{r}: unit cost of producing electric power from solar energy sources in hour $h \in \mathcal{H}$ of year $t \in \mathcal{T}$ ($\$$/kWh)
- c_{ht}^{v2g}: unit V2G electric energy cost in hour $h \in \mathcal{H}$ of year $t \in \mathcal{T}$ ($\$$/kWh)
- r_{iht}: renewable energy available at cell $i \in \mathcal{I}$ in hour $h \in \mathcal{H}$ of year $t \in \mathcal{T}$
- g_{iht}: grid power available at cell $i \in \mathcal{I}$ in hour $h \in \mathcal{H}$ of year $t \in \mathcal{T}$
- σ_{ht}: unit penalty cost for power shortage in hour $h \in \mathcal{H}$ of year $t \in \mathcal{T}$ ($\$$/kWh)
- p_t^s: minimum power demand requirement to open a charging station of year $t \in \mathcal{T}$
- p_t^b: minimum power demand requirement to open a *type 2* charging station of year $t \in \mathcal{T}$
- δ_{ht}: unit cost of storing battery in hour $h \in \mathcal{H}$ of year $t \in \mathcal{T}$
- ϕ_{ht}: unit profit of discharging battery in hour $h \in \mathcal{H}$ of year $t \in \mathcal{T}$
- q_t^{in}: number of plug-ins available for charging batteries og year $t \in \mathcal{T}$
- q_t^{out}: number of plug-ins available for discharging batteries of year $t \in \mathcal{T}$
- u_t: maximum number of batteries that can be stored at a *type 2* charging station of year $t \in \mathcal{T}$
- ρ_ω: probability of scenario $\omega \in \Omega$

Decision variables:

- Y_{ikt}: 1 if a station of type $k \in \mathcal{K}$ is opened at cell $i \in \mathcal{I}$ in year $t \in \mathcal{T}$; 0 otherwise
- $G_{iht\omega}$: amount of grid power used to satisfy demand at cell $i \in \mathcal{I}$ in hour $h \in \mathcal{H}$ of year $t \in \mathcal{T}$ under scenario $\omega \in \Omega$
- $Z_{iht\omega}$: amount of renewable power used to satisfy demand at cell $i \in \mathcal{I}$ in hour $h \in \mathcal{H}$ of year $t \in \mathcal{T}$ under scenario $\omega \in \Omega$
- $V_{iht\omega}$: amount of V2G power used to satisfy demand at cell $i \in \mathcal{I}$ in hour $h \in \mathcal{H}$ of year $t \in \mathcal{T}$ under scenario $\omega \in \Omega$
- $B_{iht\omega}$: number of batteries demands at cell $i \in \mathcal{I}$ in hour $h \in \mathcal{H}$ of year $t \in \mathcal{T}$ under scenario $\omega \in \Omega$
- $R_{iht\omega}$: amount of power shortage at cell $i \in \mathcal{I}$ in hour $h \in \mathcal{H}$ of year $t \in \mathcal{T}$ under scenario $\omega \in \Omega$
- $H_{iht\omega}$: number of full batteries stored at cell $i \in \mathcal{I}$ in hour $h \in \mathcal{H}$ of year $t \in \mathcal{T}$ under scenario $\omega \in \Omega$
- $S_{iht\omega}$: number of batteries charging at cell $i \in \mathcal{I}$ in hour $h \in \mathcal{H}$ of year $t \in \mathcal{T}$ under scenario $\omega \in \Omega$
- $P_{iht\omega}$: number of batteries discharging at cell $i \in \mathcal{I}$ in hour $h \in \mathcal{H}$ of year $t \in \mathcal{T}$ under scenario $\omega \in \Omega$

We now introduce the following first- and second-stage decision variables for our two-stage stochastic programming model. The first-stage decision variables $\mathbf{Y} \coloneqq \{Y_{ikt}\}_{i \in \mathcal{I}, k \in \mathcal{K}, t \in \mathcal{T}}$ select the type, location, and year to open a charging station as shown below:

$$Y_{ikt} = \begin{cases} 1 & \text{if a charging station of type } k \text{ is opened at cell } i \text{ in year } t \\ 0 & \text{otherwise;} \end{cases}$$

The second-stage decision variables $\mathbf{G} \coloneqq \{G_{iht\omega}\}_{i \in \mathcal{I}, h \in \mathcal{H}, t \in \mathcal{T}, \omega \in \Omega}$ denote the amount of grid power used to satisfy demand at cell $i \in \mathcal{I}$ in hour $h \in \mathcal{H}$ of year $t \in \mathcal{T}$ under scenario $\omega \in \Omega$; $\mathbf{Z} \coloneqq \{Z_{iht\omega}\}_{i \in \mathcal{I}, h \in \mathcal{H}, t \in \mathcal{T}, \omega \in \Omega}$ denote the amount of renewable power used to satisfy demand at cell $i \in \mathcal{I}$ in hour $h \in \mathcal{H}$ of year $t \in \mathcal{T}$ under scenario $\omega \in \Omega$; $\mathbf{V} \coloneqq \{V_{iht\omega}\}_{i \in \mathcal{I}, h \in \mathcal{H}, t \in \mathcal{T}, \omega \in \Omega}$ denote the amount of V2G power used to satisfy demand at cell $i \in \mathcal{I}$ in hour $h \in \mathcal{H}$ of year $t \in \mathcal{T}$ under scenario $\omega \in \Omega$; $\mathbf{B} \coloneqq \{B_{iht\omega}\}_{i \in \mathcal{I}, h \in \mathcal{H}, t \in \mathcal{T}, \omega \in \Omega}$ denote the number of batteries demand requested at cell $i \in \mathcal{I}$ in hour $h \in \mathcal{H}$ of year $t \in \mathcal{T}$ under scenario $\omega \in \Omega$; $\mathbf{H} \coloneqq \{H_{iht\omega}\}_{i \in \mathcal{I}, h \in \mathcal{H}, t \in \mathcal{T}, \omega \in \Omega}$ denote the number of full batteries available at cell $i \in \mathcal{I}$ in hour $h \in \mathcal{H}$ of year $t \in \mathcal{T}$ under scenario $\omega \in \Omega$; $\mathbf{S} \coloneqq \{S_{iht\omega}\}_{i \in \mathcal{I}, h \in \mathcal{H}, t \in \mathcal{T}, \omega \in \Omega}$ denote the number of batteries charging at cell $i \in \mathcal{I}$ in hour $h \in \mathcal{H}$ of year $t \in \mathcal{T}$ under scenario $\omega \in \Omega$; $\mathbf{P} \coloneqq \{P_{iht\omega}\}_{i \in \mathcal{I}, h \in \mathcal{H}, t \in \mathcal{T}, \omega \in \Omega}$ denote the number of batteries discharging at cell $i \in \mathcal{I}$ in hour $h \in \mathcal{H}$ of year $t \in \mathcal{T}$ under scenario $\omega \in \Omega$; and finally $\mathbf{R} \coloneqq \{R_{iht\omega}\}_{i \in \mathcal{I}, h \in \mathcal{H}, t \in \mathcal{T}, \omega \in \Omega}$ denote the amount of power shortage at cell $i \in \mathcal{I}$ in hour $h \in \mathcal{H}$ of year $t \in \mathcal{T}$ under scenario $\omega \in \Omega$.

The objective of model **[EVC]** is to minimize the first-stage and the expected value of the random second-stage costs. More specifically, the first-stage minimizes the cost of locating charging stations prior to the realization of any stochastic event (*e. g.*,

electric vehicle power demand). However, after the uncertainty is revealed, the second-stage decisions are made, which include decisions about power dispatching between charging stations and electric vehicles. These decisions depend on the first-stage decisions which are made after the uncertainties are revealed and pertain to the real-time operation. The following is a two-stage stochastic mixed-integer linear programming (MILP) model for our problem, referred to as **[EVC]**:

$$[\textbf{EVC}]\underset{\mathbf{Y}}{Minimize} \sum_{i \in \mathcal{I}} \sum_{k \in \mathcal{K}} \sum_{t \in \mathcal{T}} \psi_{ikt} Y_{ikt} + \sum_{\omega \in \Omega} \rho_\omega \mathbb{Q}\left(\mathbf{Y}, \omega\right) \tag{1}$$

subject to

$$\sum_{k \in \mathcal{K}} Y_{ikt} \leqslant 1 \quad \forall\, i \in \mathcal{I}, t \in \mathcal{T} \tag{2}$$

$$Y_{ikt-1} \leqslant Y_{ikt} \quad \forall\, i \in \mathcal{I}, k \in \mathcal{K}, t \in \mathcal{T} \tag{3}$$

$$Y_{ikt} \in \{0, 1\} \quad \forall\, i \in \mathcal{I}, k \in \mathcal{K}, t \in \mathcal{T} \tag{4}$$

with $\mathbb{Q}(\mathbf{Y}, \omega)$ being the solution of the following second-stage problem:

$$\mathbb{Q}\left(\mathbf{Y}, \omega\right) = \underset{\mathbf{G,Z,S,V,R,H,P,B}}{Minimize} \sum_{i \in \mathcal{I}} \sum_{h \in \mathcal{H}} \sum_{t \in \mathcal{T}} (c_{ht}^{pg} G_{iht\omega} + c_{ht}^{r} Z_{iht\omega} + c_{ht}^{pg} \lambda B_{iht\omega} + c_{ht}^{v2g} V_{iht\omega} +$$
$$\sigma_{ht} R_{iht\omega} + \delta_{ht} H_{iht\omega} - \phi_{ht} P_{iht\omega}) \tag{5}$$

subject to

$$G_{iht\omega} + Z_{iht\omega} + V_{iht\omega} \geqslant \sum_{k \in \mathcal{K}} p_t^s Y_{ikt} \quad \forall\, i \in \mathcal{I}, h \in \mathcal{H}, t \in \mathcal{T}, \omega \in \Omega \tag{6}$$

$$(\lambda \eta_{ht\omega} f_{iht} - (G_{iht\omega} + Z_{iht\omega} + V_{iht\omega} + \lambda B_{iht\omega})) = R_{iht\omega} \quad \forall\, i \in \mathcal{I}, h \in \mathcal{H}, t \in \mathcal{T}, \omega \in \Omega \tag{7}$$

$$max\left\{ \left\lfloor \frac{\lambda \eta_{ht\omega} f_{iht} - (g_{iht} + r_{iht} + \gamma \beta_{ht} f_{iht})}{\lambda} \right\rfloor, 0 \right\} Y_{ikt} \geqslant B_{iht\omega} \quad \forall\, i \in \mathcal{I}, h \in \mathcal{H}, k = K_2, t \in \mathcal{T}, \omega \in \Omega \tag{8}$$

$$H_{iht\omega} \leqslant u_t Y_{ikt} \quad \forall\, i \in \mathcal{I}, h \in \mathcal{H}, k = K_2, t \in \mathcal{T}, \omega \in \Omega \tag{9}$$

$$H_{iht\omega} - B_{iht\omega} - P_{iht\omega} + S_{iht\omega} = H_{i,h+1,t,\omega} \quad \forall\, i \in \mathcal{I}, h \in \mathcal{H} \backslash |H|, t \in \mathcal{T}, \omega \in \Omega \tag{10}$$

$$H_{i|H|t\omega} - B_{i|H|t\omega} - P_{i|H|t\omega} + S_{i|H|t\omega} = H_{i,1,t+1,\omega} \quad \forall\, i \in \mathcal{I}, t \in \mathcal{T} \backslash |T|, \omega \in \Omega \tag{11}$$

$$S_{i,1,1,\omega} = 0 \quad \forall\, i \in \mathcal{I}, \omega \in \Omega \tag{12}$$

$$S_{i,h+1,t,\omega} = B_{iht\omega} + P_{iht\omega} \quad \forall\, i \in \mathcal{I}, h \in \mathcal{H} \backslash |H|, t \in \mathcal{T}, \omega \in \Omega \tag{13}$$

$$S_{i,1,t+1,\omega} = B_{i|H|t\omega} + P_{i|H|t\omega} \quad \forall\, i \in \mathcal{I}, t \in \mathcal{T} \backslash |T|, \omega \in \Omega \tag{14}$$

$$S_{iht\omega} \leqslant q_t^{in} Y_{ikt} \quad \forall\, i \in \mathcal{I}, h \in \mathcal{H}, k = K_2, t \in \mathcal{T}, \omega \in \Omega \tag{15}$$

$$P_{iht\omega} \leqslant q_t^{out} Y_{ikt} \quad \forall\, i \in \mathcal{I}, h \in \mathcal{H}, k = K_2, t \in \mathcal{T}, \omega \in \Omega \tag{16}$$

$$\lambda B_{iht\omega} \geqslant p_t^b Y_{ikt} \quad \forall\, i \in \mathcal{I}, h \in \mathcal{H}, k = K_2, t \in \mathcal{T}, \omega \in \Omega \tag{17}$$

$$G_{iht\omega} \leqslant \sum_{k \in \mathcal{K}} g_{iht} Y_{ikt} \quad \forall\, i \in \mathcal{I}, h \in \mathcal{H}, t \in \mathcal{T}, \omega \in \Omega \tag{18}$$

$$V_{iht\omega} \leqslant \sum_{k \in \mathcal{K}} \gamma \beta_{ht} f_{iht} Y_{ikt} \quad \forall\, i \in \mathcal{I}, h \in \mathcal{H}, t \in \mathcal{T}, \omega \in \Omega \tag{19}$$

$$Z_{iht\omega} \leqslant \sum_{k \in \mathcal{K}} r_{iht} Y_{ikt} \quad \forall\, i \in \mathcal{I}, h \in \mathcal{H}, t \in \mathcal{T}, \omega \in \Omega \tag{20}$$

$$B_{iht\omega}, H_{iht\omega}, S_{iht\omega}, P_{iht\omega} \in Z^+ \quad \forall\, i \in \mathcal{I}, h \in \mathcal{H}, t \in \mathcal{T}, \omega \in \Omega \tag{21}$$

$$G_{iht\omega}, Z_{iht\omega}, V_{iht\omega}, R_{iht\omega} \geqslant 0 \quad \forall\, i \in \mathcal{I}, h \in \mathcal{H}, t \in \mathcal{T}, \omega \in \Omega \tag{22}$$

The objective function (1) is the sum of the first-stage costs and the expected value of the second-stage costs. The first-stage decisions minimize the annualized cost of constructing and maintaining a charging station of type $k \in \mathcal{K}$ in cell $i \in \mathcal{I}$ of year $t \in \mathcal{T}$. Constraints (2) ensure that at most one charging station of type $k \in \mathcal{K}$ is opened in a given cell $i \in \mathcal{I}$ of year $t \in \mathcal{T}$. Constraints (3) indicate that if a charging station is opened in an earlier year, it will remain open in the subsequent years. Constraints (4) set the binary restrictions for the first-stage decision variables.

The objective function in the second-stage (5) minimizes the expected value of the second-stage costs. More specifically, the first to fourth term in (5) represent the costs of charging electric vehicles due to using grid, renewable, battery, and the V2G power sources, respectively. The next two terms represent the costs associated withnot satisfying electricity demand and storing batteries in the charging stations, respectively. The last term of the objective function represents the profit associated with discharging the batteries in the charging stations. Constraints (6) mandate at least a certain amount of electricity usage p_t^s to open a charging station at a given cell $i \in \mathcal{I}$ of year $t \in \mathcal{T}$ under scenario $\omega \in \Omega$. Constraints (7) indicate that the stochastic electricity demand ($\lambda \eta_{ht\omega} f_{iht}$) at each cell $i \in \mathcal{I}$ must be satisfied either through the PG, renewable resources, V2G, swapping batteries, or through electricity purchased from other power distribution companies. Constraints (8) limit the maximum number of batters that can be demanded in a *type 2* charging station at time period $t \in \mathcal{T}$. More specifically, these constraints specify that when the three power sources (e.g., grid, renewable, and V2G) cannot satisfy the vehicles' energy demand, then the available batteries in the charging stations can be used to fulfill the vehicles' demand. Constraints (9) limit the number of batteries that can be stored in a charging station located at cell $i \in \mathcal{I}$ in hour $h \in \mathcal{H}$ of year $t \in \mathcal{T}$ under scenario $\omega \in \Omega$. Constraints (10) decide the hourly storing, charging, and discharging battery decisions for a charging station located in cell $i \in \mathcal{I}$ of a given year $t \in \mathcal{T}$ under scenario $\omega \in \Omega$. It is assumed that a battery will require an hour to be fully charged. Constraints (11) map the battery storing, charging, and discharging decisions between the last hour of the previous year to the first hour of the next year. Constraints (12) initialize that no charged batteries are available in the first hour of the first year of the planning horizon. Constraints (13) ensure that the number of batteries charged in the next hour $h + 1$ depends on the charging decisions made in the previous hour h. Constraints (14) ensure the number of batteries charged in the first hour of the next year depend upon the charging decisions taken in last hour of the previous year. Constraints (15) and (16) limit the number of batteries that can be charged and discharged in a *type 2* charging station located in cell $i \in \mathcal{I}$ at hour $h \in \mathcal{H}$ of year $t \in \mathcal{T}$ under scenario $\omega \in \Omega$. Constraints (17) set a minimum power demand p_t^b to justify opening a *type 2* charging station at cell $i \in \mathcal{I}$ of year $t \in \mathcal{T}$ under scenario $\omega \in \Omega$. Constraints (18) indicate that the amount of grid power used to satisfy electricity demand at cell $i \in \mathcal{I}$ in hour $h \in \mathcal{H}$ of year $t \in \mathcal{T}$ under scenario $\omega \in \Omega$ should not exceed their availabilities (g_{iht}). Constraints (19) indicate that the V2G power availability in a given cell $i \in \mathcal{I}$ is limited by the electric vehicles willingness to discharge at hour $h \in \mathcal{H}$ of year $t \in \mathcal{T}$ under scenario $\omega \in \Omega$. Constraints (20) limit the usage of renewable energy to the availability (r_{iht}) of a given cell $i \in \mathcal{I}$ in hour $h \in \mathcal{H}$ of year $t \in \mathcal{T}$ under scenario $\omega \in \Omega$. Finally, constraints (21) and (22) set the integrity and standard non-negativity constraints, respectively. Moreover, model [**EVC**] is extended to model [**EVE**] to ensure high renewable energy utilization which is reported in Appendix A.

3. Solution approach

An uncapacitated facility location problem (UFLP) has been shown to be NP-hard problem (Cornuejols et al., 1983). The problem addressed in this research can also be shown as a special case of the UFLP under the following conditions:

- only one time period is considered, i.e., $|\mathcal{H}| = 1$ and $|\mathcal{T}| = 1$;
- there is only one demand scenario, i.e., $|\Omega| = 1$;
- electricity demand is fulfilled primarily via the PG ($Z_{iht\omega}$ & $V_{iht\omega} = 0 \; \forall \; i \in \mathcal{I}, h \in \mathcal{H}, t \in \mathcal{T}, \omega \in \Omega$);
- there is no restriction on the PG consumption and, consequently, no power shortage;
- charging price is not dependent on the power usage in each time period ($|\mathcal{R}| = 1$); and,
- only type 1 charging station is considered, i.e., $|\mathcal{K}| = 1$. Then, no battery related activities are considered at the charging stations, i.e., $H_{iht\omega}, S_{iht\omega}, P_{iht\omega},$ & $B_{iht\omega} = 0 \; \forall \; i \in \mathcal{I}, h \in \mathcal{H}, t \in \mathcal{T}, \omega \in \Omega$.

It can be concluded that the problem investigated in this research is also strongly NP-hard problem; therefore, there is no guarantee of solving this problem to optimally in a polynomial time. Consequently, commercial solvers, such as CPLEX/GUROBI, will fail to solve any large instance of such problems. To overcome these computational challenges, we propose a hybrid decomposition algorithm that combines Sample Average Approximation technique with an enhanced Progressive Hedging Algorithm. The techniques used to enhance the Progressive Hedging Algorithm are local and global adjustment techniques, and few variants of the rolling horizon algorithm. Interested reader is referred to review the recent study by Poudel et al. (2017) for the details about this hybrid sampling based decomposition algorithm. The aim is to efficiently generate high-quality feasible solutions for our problem [**EVC**].

3.1. Sample average approximation

The percentage of electric vehicles $\eta_{ht\omega}$ that require charging in a charging station located at cell $i \in \mathcal{I}$ in hour $h \in \mathcal{H}$ of year $t \in \mathcal{T}$ differs significantly from one hour to the next of a given year. It mandates evaluating a large scenario set to provide meaningful insights for the decision makers. However, evaluating such a large scenario set poses significant computational challenges in solving model [**EVC**]. To remedy this problem, a sampling technique, commonly known as the *Sample Average Approximation* (SAA) method, is employed to reduce the computational burden associated with solving model [**EVC**] in a timely fashion. The SAA has been extensively used previously to solve many large scale network flow related problems, such as Quddus et al. (2018),Marino et al. (2018), Quddus et al. (2018), and others. Interested readers may review the work by Kleywegt et al. (2001) to understand the convergence properties of the SAA technique. In SAA, a sample $\omega^1, \omega^2, \ldots, \omega^N$ of N realization of the random vector ω is generated from Ω (where $N < |\Omega|$) according a normal probability distribution $\mathbb{P}$, and they are solved repeatedly until a pre-specified tolerance gap is achieved. Problem [**EVC**] is now approximated by the following SAA problem:

$$\underset{Y \in \mathbf{Y}}{Minimize} \left\{ \mathbf{v}_N^m := \sum_{i \in \mathcal{I}} \sum_{k \in \mathcal{K}} \sum_{t \in \mathcal{T}} \psi_{ikt} Y_{ikt} + \frac{1}{N} \sum_{n=1}^{N} \mathbb{Q}\left(\mathbf{Y}, n \right) \right\} \tag{23}$$

As the sample size increases, the optimal solution of (23) converges with probability one to an optimal solution of the original problem [**EVC**] (Kleywegt et al., 2001). Assuming that the SAA problem is solved within an absolute optimality gap $\delta \geqslant 0$, we can estimate the sample size N needed to guarantee an ϵ-optimal solution to the true problem with probability at least equal to $(1 - \alpha)$ as:

$$N \geqslant \frac{3\sigma_{max}^2}{(\epsilon - \delta)^2} (|\mathcal{I}||\mathcal{K}||\mathcal{T}|(log 2) - log \alpha) \tag{24}$$

where $\epsilon > \delta$, $\alpha \in (0, 1)$, and σ_{max}^2 is a maximal variance of certain function differences (Kleywegt et al., 2001). In each iteration of the algorithmic step, SAA provides a valid statistical lower and upper bound for the original problem [**EVC**], and the process terminates when the gap between the estimators falls below a pre-specified threshold value. The main steps to solve [**EVC**] using the Sample Average Approximation (SAA) approach are explained below:

Step 1: Generate M independent percentage of electric vehicle recharging scenarios of size N $i.e.$,
$\{\boldsymbol{\eta}_m^1(\omega), \boldsymbol{\eta}_m^2(\omega), ..., \boldsymbol{\eta}_m^N(\omega)\}$; $\forall$ $m = 1, ..., M$, where $\boldsymbol{\eta} = \{\eta_{ht\omega}$; $\forall$ $h \in \mathcal{H}, t \in \mathcal{T}, \omega \in \Omega\}$ and solve the corresponding SAA problem (25). Each sample consists of N realizations of independently and identically distributed ($i. i. d.$) random scenarios.

$$\underset{Y \in \mathbf{Y}}{Minimize} \left\{ \mathbf{v}_N^m := \sum_{i \in \mathcal{I}} \sum_{k \in \mathcal{K}} \sum_{t \in \mathcal{T}} \psi_{ikt} Y_{ikt} + \frac{1}{N} \sum_{n=1}^{N} \mathbb{Q}\left(\mathbf{Y}, n \right) \right\} \tag{25}$$

The optimal objective value is denoted by $\mathbf{v}_N^m$ and the optimal solution by $\hat{\mathbf{Y}}_N^m$; $m = 1, ..., M$.
Step 2: Compute the average of the optimal solutions obtained by solving all SAA problems, $\bar{\mathbf{v}}_M^N$ and variance, $\sigma_{\bar{\mathbf{v}}_M^N}^2$:

$$\bar{\mathbf{v}}_M^N = \frac{1}{M} \sum_{m=1}^{M} \mathbf{v}_N^m \tag{26}$$

where $\bar{\mathbf{v}}_M^N$ provides a statistical lower bound on the optimal objective function value ($\mathbf{v}^*$) for the original problem defined by Eqs. (1)–(22) $i. e.$, $\bar{\mathbf{v}}_M^N \leqslant \mathbf{v}^*$. Since M samples are generated and $\mathbf{v}_N^1, \mathbf{v}_N^2, ..., \mathbf{v}_N^M$ are independent, the variance of $\bar{\mathbf{v}}_M^N$ is given by:

$$\sigma_{\bar{\mathbf{v}}_M^N}^2 = \frac{1}{(M - 1)M} \sum_{m=1}^{M} (\mathbf{v}_N^m - \bar{\mathbf{v}}_M^N)^2 \tag{27}$$

Step 3: Pick a feasible first-stage solution $\widetilde{Y} \in \mathbf{Y}$ obtained from **Step 1** of the SAA algorithm, $i. e.$, one of the solutions from $\hat{\mathbf{Y}}_N^m$ and estimate the objective function value of the original problem using a reference sample N' as follows:

$$\widetilde{\mathbf{g}}_{N'}(\widetilde{Y}) := \sum_{i \in \mathcal{I}} \sum_{k \in \mathcal{K}} \sum_{t \in \mathcal{T}} \psi_{ikt} Y_{ikt} + \frac{1}{N'} \sum_{n=1}^{N'} \mathbb{Q}\left(\mathbf{Y}, n \right) \tag{28}$$

The estimator $\widetilde{\mathbf{g}}_{N'}(\widetilde{Y})$ serves as an upper bound for the optimal objective function value of problem [**EVC**]. Typically, sample size N' is chosen much larger than the sample size N in the SAA problems $i. e.$, $N' \gg N$ (Kleywegt et al., 2001). We can estimate the variance of $\widetilde{\mathbf{g}}_{N'}(\widetilde{Y})$ as follows:

$$\sigma_{N'}^2(\widetilde{Y}) = \frac{1}{(N' - 1)N'} \sum_{n=1}^{N'} \left\{ \sum_{i \in \mathcal{I}} \sum_{k \in \mathcal{K}} \sum_{t \in \mathcal{T}} \psi_{ikt} \widetilde{Y}_{ikt} + \mathbb{Q}\left(\mathbf{Y}, n \right) - \widetilde{\mathbf{g}}_{N'}(\widetilde{Y}) \right\}^2$$

where $\mathbb{Q}(\mathbf{Y}, n)$ represents the solution of the second-stage problem.
Step 4: Compute the optimality gap ($gap_{N,M,N'}(\widetilde{Y})$) and its variance ($\sigma_{gap}^2$) using the estimators calculated in **Steps 2** and **3**.

$$gap_{N,M,N'}(\widetilde{Y}) = \widetilde{\mathbf{g}}_{N'}(\widetilde{Y}) - \bar{\mathbf{v}}_M^N$$
$$\sigma_{gap}^2 = \sigma_{N'}^2(\widetilde{Y}) + \sigma_{\bar{\mathbf{v}}_M^N}^2$$

The confidence interval for the optimality gap is then calculated as follows:

$$\widetilde{\mathbf{g}}_{N'}(\widetilde{Y}) - \bar{\mathbf{v}}_M^N + z_\alpha \{\sigma_{N'}^2(\widetilde{Y}) + \sigma_{\bar{\mathbf{v}}_M^N}^2\}^{1/2}$$

with $z_\alpha := \Phi^{-1}(1 - \alpha)$, where $\Phi(z)$ is the cumulative distribution function of the standard normal distribution.

3.2. Progressive Hedging algorithm

In **Step1**, the SAA algorithm requires to solve a two-stage stochastic mixed-integer programming model consisting of N scenarios. Depending on the size of $|\mathcal{I}|$, $|\mathcal{K}|$, and $|\mathcal{T}|$, which significantly impacts the computational performance of the SAA problems, problem (25) can still be considered challenging. Often, decomposition based methods can be employed to divide the original problem into smaller and more manageable subproblems (Rockafellar and Wets, 1991). This motivates us to solve each subproblem of the SAA problem using a Progressive Hedging Algorithm (PHA). The PHA offers high-quality solutions in solving a variety of application-specific problems. An example of such can be found in (Huang et al., 2014; Quddus et al., 2019; Quddus, 2018), and many others.

Constraints (6) ((8) ((9) (), (and), (16)–(19), ()) in [**EVC**] link the first-stage decisions with the second-stage decision variables. Therefore, these constraints do not allow problem (25) to be separable by scenarios. To remedy this problem, we created a copy variable $\{Y_{ikt}^n\}_{\forall i \in I, k \in \mathcal{K}, t \in \mathcal{T}, n \in \mathcal{N}} \in \{0, 1\}$ which ensures that the copy of the first-stage decision variables are created for each scenario $n \in N$. Problem (25) can now be rewritten as follows:

$$\underset{\mathbf{Y,G,Z,S,V,R,H,P,B}}{Minimize} \sum_{n=1}^{N} \sum_{i \in I} \sum_{t \in \mathcal{T}} \frac{1}{N} \left\{ \sum_{k \in \mathcal{K}} \psi_{ikt} Y_{ikt}^n + \sum_{h \in \mathcal{H}} (c_{ht}^{pg} G_{ihtn} + c_{ht}^r Z_{ihtn} + c_{ht}^{pg} \lambda B_{ihtn} + c_{ht}^{v2g} V_{ihtn} + \right.$$
$$\left. \sigma_{ht} R_{ihtn} + \delta_{ht} H_{ihtn} - \phi_{ht} P_{ihtn}) \right\}$$

subject to: (7), (10)–(14), (21), (22) and

$$\sum_{k \in \mathcal{K}} Y_{ikt}^n \leqslant 1 \quad \forall i \in \mathcal{I}, t \in \mathcal{T}, n \in \mathcal{N} \tag{29}$$

$$Y_{ikt-1}^n \leqslant Y_{ikt}^n \quad \forall i \in \mathcal{I}, k \in \mathcal{K}, t \in \mathcal{T}, n \in \mathcal{N} \tag{30}$$

$$G_{ihtn} + Z_{ihtn} + V_{ihtn} \geqslant \sum_{k \in \mathcal{K}} p_t^s Y_{ikt}^n \quad \forall i \in \mathcal{I}, h \in \mathcal{H}, t \in \mathcal{T}, n \in \mathcal{N} \tag{31}$$

$$max \left\{ \left\lfloor \frac{\lambda \eta_{htn} f_{iht} - (g_{iht} + r_{iht} + \gamma \beta_{ht} f_{iht})}{\lambda} \right\rfloor, 0 \right\} Y_{ikt}^n \geqslant B_{ihtn} \quad \forall i \in \mathcal{I}, h \in \mathcal{H}, k = K_2, t \in \mathcal{T}, n \in \mathcal{N} \tag{32}$$

$$H_{ihtn} \leqslant u_t Y_{ikt}^n \quad \forall i \in \mathcal{I}, h \in \mathcal{H}, k = K_2, t \in \mathcal{T}, n \in \mathcal{N} \tag{33}$$

$$S_{ihtn} \leqslant q_t^{in} Y_{ikt}^n \quad \forall i \in \mathcal{I}, h \in \mathcal{H}, k = K_2, t \in \mathcal{T}, n \in \mathcal{N} \tag{34}$$

$$P_{ihtn} \leqslant q_t^{out} Y_{ikt}^n \quad \forall i \in \mathcal{I}, h \in \mathcal{H}, k = K_2, t \in \mathcal{T}, n \in \mathcal{N} \tag{35}$$

$$\lambda B_{ihtn} \geqslant p_t^b Y_{ikt}^n \quad \forall i \in \mathcal{I}, h \in \mathcal{H}, k = K_2, t \in \mathcal{T}, n \in \mathcal{N} \tag{36}$$

$$G_{ihtn} \leqslant \sum_{k \in \mathcal{K}} g_{iht} Y_{ikt}^n \quad \forall i \in \mathcal{I}, h \in \mathcal{H}, t \in \mathcal{T}, n \in \mathcal{N} \tag{37}$$

$$V_{ihtn} \leqslant \sum_{k \in \mathcal{K}} \gamma \beta_{ht} f_{iht} Y_{ikt}^n \quad \forall i \in \mathcal{I}, h \in \mathcal{H}, t \in \mathcal{T}, n \in \mathcal{N} \tag{38}$$

$$Z_{ihtn} \leqslant \sum_{k \in \mathcal{K}} r_{iht} Y_{ikt}^n \quad \forall i \in \mathcal{I}, h \in \mathcal{H}, t \in \mathcal{T}, n \in \mathcal{N} \tag{39}$$

$$Y_{ikt}^n = Y_{ikt}^q \quad \forall n, q \in N, n \neq q \tag{40}$$

$$Y_{ikt}^n \in \{0, 1\} \quad \forall i \in \mathcal{I}, k \in \mathcal{K}, t \in \mathcal{T}, n \in \mathcal{N} \tag{41}$$

Constraints (40) are referred to as *nonanticipativity* constraints. These constraints link the first- and second-stage decision variables and force all scenarios to yield the same first-stage decision variables. To make the model separable by scenarios and to apply Lagrangian relaxation, we need to rewrite the *nonanticipativity* constraints. Let $\{\overline{Y}_{ikt}\}_{\forall i \in I, k \in \mathcal{K}, t \in \mathcal{T}} \in \{0, 1\}$ be the "overall design vector." The following constraints are equivalent to (40):

$$Y_{ikt}^n = \overline{Y}_{ikt} \quad \forall i \in \mathcal{I}, k \in \mathcal{K}, t \in \mathcal{T}, n \in \mathcal{N} \tag{42}$$

$$\overline{Y}_{ikt} \in \{0, 1\} \quad \forall i \in \mathcal{I}, k \in \mathcal{K}, t \in \mathcal{T} \tag{43}$$

We employ the augmented Lagrangian strategy, proposed by Rockafellar and Wets (1991), to relax constraints (42) and obtain the following objective function:

$$\underset{\mathbf{Y,G,Z,S,V,R,H,P,B}}{Minimize} \sum_{n=1}^{N} \sum_{i \in \mathcal{I}} \sum_{t \in \mathcal{T}} \frac{1}{N} \left\{ \sum_{k \in \mathcal{K}} \psi_{ikt} Y_{ikt}^n + \sum_{h \in \mathcal{H}} (c_{ht}^{pg} G_{ihtn} + c_{ht}^r Z_{ihtn} + c_{ht}^{pg} \lambda B_{ihtn} + c_{ht}^{v2g} V_{ihtn} + \right.$$

$$\left. \sigma_{ht} R_{ihtn} + \delta_{ht} H_{ihtn} - \phi_{ht} P_{ihtn}) + \sum_{k \in \mathcal{K}} \xi_{ikt}^n \left(Y_{ikt}^n - \overline{Y}_{ijt} \right) + \frac{1}{2} \sum_{k \in \mathcal{K}} \pi (Y_{ikt}^n - \overline{Y}_{ikt})^2 \right\}$$

where $\{\xi_{ikt}^n\}_{\forall i \in \mathcal{I}, k \in \mathcal{K}, t \in \mathcal{T}, n \in \mathcal{N}}$ defines the Lagrangian multipliers for the relaxed constraints and π defines a penalty ratio. Given the binary requirements of variables $\{Y_{ikt}^n\}_{\forall i \in \mathcal{I}, k \in \mathcal{K}, t \in \mathcal{T}, n \in \mathcal{N}}$ and $\{\overline{Y}_{ikt}\}_{\forall i \in \mathcal{I}, k \in \mathcal{K}, t \in \mathcal{T}}$, the quadratic term $\sum_{i \in \mathcal{I}} \sum_{k \in \mathcal{K}} \sum_{t \in \mathcal{T}} \pi (Y_{ikt}^n - \overline{Y}_{ikt})^2$ shown in the above objective function can be reduced as follows:

$$\sum_{i \in \mathcal{I}} \sum_{k \in \mathcal{K}} \sum_{t \in \mathcal{T}} \pi (Y_{ikt}^n - \overline{Y}_{ikt})^2 = \sum_{i \in \mathcal{I}} \sum_{k \in \mathcal{K}} \sum_{t \in \mathcal{T}} (\pi (Y_{ikt}^n)^2 - 2\pi Y_{ikt}^n \overline{Y}_{ikt} + \pi (\overline{Y}_{ikt})^2)$$

$$= \sum_{i \in \mathcal{I}} \sum_{k \in \mathcal{K}} \sum_{t \in \mathcal{T}} (\pi Y_{ikt}^n - 2\pi Y_{ikt}^n \overline{Y}_{ikt} + \pi \overline{Y}_{ikt})$$

Meanwhile, the objective function can be reduced as follows:

$$\underset{\mathbf{Y,G,Z,S,V,R,H,P,B}}{Minimize} \sum_{n=1}^{N} \sum_{i \in \mathcal{I}} \sum_{t \in \mathcal{T}} \frac{1}{N} \left\{ \sum_{k \in \mathcal{K}} \left(\psi_{ikt} + \xi_{ikt}^n - \pi \overline{Y}_{ikt} + \frac{\pi}{2} \right) Y_{ikt}^n + \sum_{h \in \mathcal{H}} (c_{ht}^{pg} G_{ihtn} + c_{ht}^r Z_{ihtn} + \right.$$

$$\left. c_{ht}^{pg} \lambda B_{ihtn} + c_{ht}^{v2g} V_{ihtn} + \sigma_{ht} R_{ihtn} + \delta_{ht} H_{ihtn} - \phi_{ht} P_{ihtn}) - \sum_{k \in \mathcal{K}} \xi_{ikt}^n \overline{Y}_{ikt} + \frac{1}{2} \sum_{k \in \mathcal{K}} \pi \overline{Y}_{ikt} \right\}$$

When the value of the overall plan $\{\overline{Y}_{ikt}\}_{\forall i \in \mathcal{I}, k \in \mathcal{K}, t \in \mathcal{T}}$ is fixed, the last two terms of the above objective function become constant and can be removed from the objective function. This will allow the subproblems to be decomposable by scenarios $n \in N$. The overall problem can be formulated for each scenario $n \in \mathcal{N}$ as follows:

$$[\mathbf{EVC}](\mathbf{PHA}) \underset{\mathbf{Y,G,Z,S,V,R,H,P,B}}{Minimize} \sum_{i \in \mathcal{I}} \sum_{t \in \mathcal{T}} \left\{ \sum_{k \in \mathcal{K}} \left(\psi_{ikt} + \xi_{ikt}^n - \pi \overline{Y}_{ikt} + \frac{\pi}{2} \right) Y_{ikt}^n + \sum_{h \in \mathcal{H}} (c_{ht}^{pg} G_{ihtn} + \right.$$

$$\left. c_{ht}^r Z_{ihtn} + c_{ht}^{pg} \lambda B_{ihtn} + c_{ht}^{v2g} V_{ihtn} + \sigma_{ht} R_{ihtn} + \delta_{ht} H_{ihtn} - \phi_{ht} P_{ihtn}) \right\}$$

subject to

$$\sum_{k \in \mathcal{K}} Y_{ikt}^n \leqslant 1 \quad \forall i \in \mathcal{I}, t \in \mathcal{T} \tag{44}$$

$$Y_{ikt-1}^n \leqslant Y_{ikt}^n \quad \forall i \in \mathcal{I}, k \in \mathcal{K}, t \in \mathcal{T} \tag{45}$$

$$G_{ihtn} + Z_{ihtn} + V_{ihtn} \geqslant \sum_{k \in \mathcal{K}} p_t^s Y_{ikt}^n \quad \forall i \in \mathcal{I}, h \in \mathcal{H}, t \in \mathcal{T} \tag{46}$$

$$(\lambda \eta_{htn} f_{iht} - (G_{ihtn} + Z_{ihtn} + V_{ihtn} + \lambda B_{ihtn})) = R_{ihtn} \quad \forall i \in \mathcal{I}, h \in \mathcal{H}, t \in \mathcal{T} \tag{47}$$

$$max \left\{ \left\lfloor \frac{\lambda \eta_{htn} f_{iht} - (g_{iht} + r_{iht} + \gamma \beta_{ht} f_{iht})}{\lambda} \right\rfloor, 0 \right\} Y_{ikt}^n \geqslant B_{ihtn} \quad \forall i \in \mathcal{I}, h \in \mathcal{H}, k = K_2, t \in \mathcal{T} \tag{48}$$

$$H_{ihtn} \leqslant u_t Y_{ikt}^n \quad \forall i \in \mathcal{I}, h \in \mathcal{H}, k = K_2, t \in \mathcal{T} \tag{49}$$

$$H_{ihtn} - B_{ihtn} - P_{ihtn} + S_{ihtn} = H_{i,h+1,t,n} \quad \forall i \in \mathcal{I}, h \in \mathcal{H} \backslash |H|, t \in \mathcal{T} \tag{50}$$

$$H_{i|H|tn} - B_{i|H|tn} - P_{i|H|tn} + S_{i|H|tn} = H_{i,1,t+1,n} \quad \forall i \in \mathcal{I}, t \in \mathcal{T} \backslash |T| \tag{51}$$

$$S_{i,1,1,n} = 0 \quad \forall i \in \mathcal{I} \tag{52}$$

$$S_{i,h+1,t,n} = B_{ihtn} + P_{ihtn} \quad \forall i \in \mathcal{I}, h \in \mathcal{H} \backslash |H|, t \in \mathcal{T} \tag{53}$$

$$S_{i,1,t+1}^n = B_{i|H|t}^n + P_{i|H|t}^n \quad \forall i \in \mathcal{I}, t \in \mathcal{T} \backslash |T| \tag{54}$$

$$S_{ihtn} \leqslant q_t^{in} Y_{ikt}^n \quad \forall i \in \mathcal{I}, h \in \mathcal{H}, k = K_2, t \in \mathcal{T} \tag{55}$$

$$P_{ihtn} \leqslant q_t^{out} Y_{ikt}^n \quad \forall i \in \mathcal{I}, h \in \mathcal{H}, k = K_2, t \in \mathcal{T} \tag{56}$$

$$\lambda B_{ihtn} \geqslant p_t^b Y_{ikt}^n \quad \forall i \in \mathcal{I}, h \in \mathcal{H}, k = K_2, t \in \mathcal{T} \tag{57}$$

$$G_{ihtn} \leqslant \sum_{k \in \mathcal{K}} g_{iht} Y_{ikt}^n \quad \forall i \in \mathcal{I}, h \in \mathcal{H}, t \in \mathcal{T} \tag{58}$$

$$V_{ihtn} \leqslant \sum_{k \in \mathcal{K}} \gamma \beta_{ht} f_{iht} Y_{ikt}^n \quad \forall\, i \in \mathcal{I},\, h \in \mathcal{H},\, t \in \mathcal{T} \tag{59}$$

$$Z_{ihtn} \leqslant \sum_{k \in \mathcal{K}} r_{iht} Y_{ikt}^n \quad \forall\, i \in \mathcal{I},\, h \in \mathcal{H},\, t \in \mathcal{T} \tag{60}$$

$$Y_{ikt}^n \in \{0, 1\} \quad \forall\, i \in \mathcal{I},\, k \in \mathcal{K},\, t \in \mathcal{T} \tag{61}$$

$$B_{ihtn}, H_{ihtn}, S_{ihtn}, P_{ihtn} \in Z^+ \quad \forall\, i \in \mathcal{I},\, h \in \mathcal{H},\, t \in \mathcal{T} \tag{62}$$

$$G_{ihtn}, Z_{ihtn}, V_{ihtn}, R_{ihtn} \geqslant 0 \quad \forall\, i \in \mathcal{I},\, h \in \mathcal{H},\, t \in \mathcal{T} \tag{63}$$

Here, $\{\xi_{ikt}^{n,r}\}_{\forall i \in \mathcal{I}, k \in \mathcal{K}, t \in \mathcal{T}, n \in \mathcal{N}}$ and π^r denote the lagrangian multipliers and penalty parameter of the PHA, respectively, which are updated at each iteration r. The values of $\xi_{ikt}^{n,r}$ and π^r are updated using Eqs. (64) and (65) and the process continues.

$$\xi_{ikt}^{n,r} \leftarrow \xi_{ikt}^{n,r-1} + \pi^{r-1}(Y_{ikt}^{n,r} - \overline{Y}_{ikt}^{r-1}) \quad \forall\, i \in \mathcal{I},\, k \in \mathcal{K},\, t \in \mathcal{T} \tag{64}$$

$$\pi^r \leftarrow \alpha \pi^{r-1} \tag{65}$$

where α is a given constant which we initialize at $\alpha > 1$. We further initialize $\xi_{lkt}^{n,0} \leftarrow 0$;$\forall\, l \in \mathcal{L},\, k \in \mathcal{K},\, t \in \mathcal{T},\, n \in N$. Finally, π^0 is set to a fixed positive value to ensure that $\pi^r \to \infty$ as the number of iterations r increases. A Pseudo-code of the basic PHA is provided in Algorithm 1.

Termination Criteria: The PHA terminates when one of the following conditions is satisfied:

- $\frac{1}{N} \sum_{n=1}^N \sum_{i \in \mathcal{I}} \sum_{k \in \mathcal{K}} \sum_{t \in \mathcal{T}} |Y_{ikt}^{n,r} - \overline{Y}_{ikt}^r| \leqslant \epsilon$; where ϵ is a pre-specified tolerance gap
- 10 consecutive non-improvement iterations
- Maximum iteration limit is reached (*i. e.*, $iter^{max} = 100$)
- Maximum time limit is reached (*i. e.*, $time^{max} = 10{,}800$ CPU seconds)

Algorithm 1. Progressive Hedging algorithm

Initialize, $r \leftarrow 1$, ϵ, $\{\xi_{ikt}^{n,r}\}_{\forall i \in \mathcal{I}, k \in \mathcal{K}, t \in \mathcal{T}, n \in \mathcal{N}} \leftarrow 0$, $\pi^r \leftarrow \pi^0$
terminate←**false**
while (*terminate*=**false**) **do**
  for $n = 1$ to N
    Solve [**EVC**(**PHA**)] and obtain $\{Y_{ikt}^{n,r}\}_{\forall i \in \mathcal{I}, k \in \mathcal{K}, t \in \mathcal{T}, n \in \mathcal{N}}$
  end for
  Calculate the consensus parameter:
    $\overline{Y}_{ikt}^r \leftarrow \frac{1}{N} \sum_{n=1}^N Y_{ikt}^{n,r}$;$\forall\, i \in \mathcal{I},\, k \in \mathcal{K},\, t \in \mathcal{T}$
  if ($r > 1$) **then**
    Update the largangian parameter:
      $\xi_{ikt}^{n,r} \leftarrow \xi_{ikt}^{n,r-1} + \pi^{r-1}(Y_{ikt}^{n,r} - \overline{Y}_{ikt}^{r-1})$;$\forall\, i \in \mathcal{I},\, k \in \mathcal{K},\, t \in \mathcal{T}$
    Update the penalty parameter:
      $\pi^r \leftarrow \alpha \pi^{r-1}$ and $\alpha > 1$
  end if
  if $\left((Y_{ikt}^{n,r} - \overline{Y}_{ikt}^{r-1})_{\forall i \in \mathcal{I}, k \in \mathcal{K}, t \in \mathcal{T}} \leqslant \epsilon \right)$ **then**
    terminate←**true**
  end if
  $r \leftarrow r + 1$
end while

3.3. Enhanced Progressive Hedging algorithm

Even though the PHA shows faster convergence in solving small to medium sized network problems, the technique fails to provide a reasonable solution for sufficiently large sized network design problems. This motivates us to explore additional enhancement techniques (*e. g.*, local and global heuristics, dynamic penalty parameter updating technique, different variants of the rolling horizon heuristic) to further improve the convergence and stability of the basic Progressive Hedging Algorithm. The following subsection discusses some PHA enhancement techniques that we have investigated in an attempt to make the model [**EVC**(**PHA**)] solve faster.

3.3.1. Penalty parameter updating

Prior studies, such as Huang et al. (2014), show that the performance of the PHA is significantly impacted by choosing an appropriate π value. For instance, the algorithm converges faster to a sub-optimal solution for a significantly large value of π. However, the algorithm takes a longer time to converge if π is set to a conservative value. Since there is no way we can estimate the

appropriate π value for a given optimization problem in advance, we adopt the strategies proposed by Hvattum and Lokketangen (2009) to dynamically adjust the value of π over iterations based on the computational performance obtained from prior iterations of the PHA algorithm. Let Δ_1^r and Δ_2^r define the indicators of the convergence rates in the dual and primal space, respectively. The penalty value can now be updated as follows:

$$\Delta_1^r = \sum_{i \in \mathcal{I}} \sum_{k \in \mathcal{K}} \sum_{t \in \mathcal{T}} (Y_{ikt}^r - \overline{Y}_{ikt}^r)^2 \tag{66}$$

$$\Delta_2^r = \sum_{i \in \mathcal{I}} \sum_{k \in \mathcal{K}} \sum_{t \in \mathcal{T}} (\overline{Y}_{ikt}^r - \overline{Y}_{ikt}^{r-1})^2 \tag{67}$$

$$\pi^r = \begin{cases} \varphi \pi^{r-1} & \text{if } \Delta_1^r - \Delta_1^{r-1} > 0 \\ \frac{1}{\varphi} \pi^{r-1} & \text{elseif } \Delta_2^r - \Delta_2^{r-1} > 0 \\ \pi^{r-1} & \text{otherwise} \end{cases} \tag{68}$$

where φ is a constant parameter whose value is set to $\varphi > 1$.

3.3.2. Heuristic strategies

We will now employ two heuristic strategies, proposed by Crainic et al. (2011), that modify the value of ψ_{ikt} in problem [**EVC**(**PHA**)] to further enhance the performance of the Progressive Hedging Algorithm. The first is termed *global heuristic* as this strategy adjusts the value of ψ_{ikt} at the end of each iteration r. On the other hand, the second, referred to as *local heuristic*, adjusts the value of ψ_{ikt} within the scenario level.

We realize that problem [**EVC**(**PHA**)] can be decomposed into N deterministic sub-problems. At the end of each iteration r of Algorithm 1, we can obtain the values of the consensus parameter $\{\overline{Y}_{ikt}^r\}_{\forall i \in \mathcal{I}, k \in \mathcal{K}, t \in \mathcal{T}}$ which provides an indication of how many times a charging station of type $k \in \mathcal{K}$ is opened in cell $i \in \mathcal{I}$ of year $t \in \mathcal{T}$ in the previous iterations. A higher value of $\overline{Y}_{ikt}^r$ means that the charging station of type $k \in \mathcal{K}$ located in cell $i \in \mathcal{I}$ at year $t \in \mathcal{T}$ was selected in many of the previous iterations. Contrarily, a lower value of $\overline{Y}_{ikt}^r$ indicates that a charging station of type $k \in \mathcal{K}$ opened in cell $i \in \mathcal{I}$ at year $t \in \mathcal{T}$ was not a favorable decision in most of the previous iterations. Let $\overline{a}$ and $\underline{a}$ be the two parameters that define the upper and lower threshold values. Therefore, if the value of $\overline{Y}_{ikt}^r$ is greater than the threshold value $\overline{a}$, then lowering the fixed cost of opening a charging station will attract the subproblems to use that charging station in the coming iterations. Similarly, if the value of $\overline{Y}_{ikt}^r$ is lower than the threshold value $\underline{a}$, then increasing the fixed cost of opening a charging station will discourage the use of that charging station in the subproblems of the coming iterations. This will fix the decisions of using fewer charging stations in a given year to either one or zero and thus will help reduce the size of the problem. The adjustment strategy is shown as follows:

$$\psi_{ikt}^r = \begin{cases} \kappa \psi_{ikt}^{r-1} & \text{if } \overline{Y}_{ikt}^{r-1} < \underline{a} \\ \frac{1}{\kappa} \psi_{ikt}^{r-1} & \text{if } \overline{Y}_{ikt}^{r-1} > \overline{a} \\ \psi_{ikt}^{r-1} & \text{Otherwise} \end{cases} \tag{69}$$

where ψ_{ikt}^r represents the modified fixed cost of opening a charging station of type $k \in \mathcal{K}$ at cell $i \in \mathcal{I}$ in year $t \in \mathcal{T}$ and iteration r; $\underline{a}$ and $\overline{a}$ are the two constant parameters whose values are set to $0 < \underline{a} < 0.3$ and $0.7 < \overline{a} < 1$; and κ is a constant parameter whose value is set to $\kappa > 1$.

We can further enhance the *global heuristic* strategy by modifying the selection of ψ_{ikt} locally within the scenario level. This strategy is termed as *local heuristic* (Crainic et al., 2011) since the modification of ψ_{ikt} only impacts the subproblem of the current scenario n at a particular iteration r. This strategy emphasizes on modifying the cost associated with opening a charging station of type $k \in \mathcal{K}$ at cell $i \in \mathcal{I}$ in year $t \in \mathcal{T}$ under scenario $n \in N$ if the gap between $Y_{ikt}^{n,r}$ and $\overline{Y}_{ikt}^r$ is sufficiently large in a given iteration r. The local adjustment strategy is then applied to Algorithm 1 as follows:

$$\psi_{ikt}^{n,r} = \begin{cases} \kappa \psi_{ikt}^r & \text{if } |Y_{ikt}^{n,r-1} - \overline{Y}_{ikt}^r| \geqslant a^{far} \text{ and } Y_{ikt}^{n,r-1} = 1 \\ \frac{1}{\kappa} \psi_{ikt}^r & \text{if } |Y_{ikt}^{n,r-1} - \overline{Y}_{ikt}^r| \geqslant a^{far} \text{ and } Y_{ikt}^{n,r-1} = 0 \\ \psi_{ikt}^r & \text{Otherwise} \end{cases} \tag{70}$$

where $\psi_{ikt}^{n,r}$ represents the modified ψ_{ikt} of opening a charging station of type $k \in \mathcal{K}$ at cell $i \in \mathcal{I}$ in year $t \in \mathcal{T}$ under scenario $n \in N$ and at iteration r; a^{far} is a threshold point at which a local adjustment to the ψ_{ikt} of selecting a cell is applied and is set to $0.5 < a^{far} < 1$; and κ is a constant parameter whose value is set to $\kappa > 1$.

3.3.3. Rolling Horizon Heuristic Strategy

The PHA algorithm demonstrates high-computational capability in solving small- to medium-size problems. However, PHA is not capable of providing a reasonable solution for large-size problems. This motivates us to explore additional enhancement techniques with different variants of the Rolling Horizon Heuristic strategy to further improve the convergence and stability of the PHA algorithm, i.e., solving sub-problems faster.

It is worth noting that the Progressive Hedging Algorithm still requires solving a deterministic, multi-period problem [**EVC(PHA)**] N times, which is still considered challenging from a solution standpoint. One way to tackle this problem is to split the

planning horizon (i.e., years and hours) into multiple slices and solve them sequentially until all the slices are investigated. In this study, we employ a *Rolling Horizon* (RH) heuristic that decomposes problem **[EVC(PHA)]** into a series of small sub-problems. This is made for a few consecutive hour-year combinations from the overall planning horizon. The algorithm terminates when all the hour-year combinations of the planning horizon are investigated. Interested readers can review the studies conducted by Balasubramanian and Grossmann (2004) and Poudel et al. (2018) to learn more about the RH heuristic.

Three different variants of the RH heuristic are proposed to find high-quality solutions to solve problem **[EVC(PHA)]** in a reasonable amount of time. The first variant of the RH heuristic, i.e., **[RH1]**, decomposes problem **[EVC(PHA)]** on yearly basis, while the second and third variants of the RH heuristic, i.e., **[RH2]** and **[RH3]**, respectively, decompose problem **[EVC(PHA)]** on hourly and a combination of hourly and yearly bases, respectively. A pseudo-code of the basic RH heuristic is provided in Algorithm 2.

Algorithm 2. Rolling Horizon Heuristic

Input: Termination criteria: $iter^{max}$, $time^{max}$, and ϵ;
Output: Upper bound $z(Y^r_{ikt})$;
Step 1: Initialize: $r \leftarrow 1$, $t^r_0 \leftarrow 0$, $h^r_0 \leftarrow 0$, M^r, Q^r ;
$terminate \leftarrow false$;
while $(terminate = false)$ **do**
    Set:
       • $Y^n_{ikt} \in \{0, 1\}$ and $B_{ihtn}, H_{ihtn}, S_{ihtn}, P_{ihtn} \in \mathbb{Z}^+$ for $t^r_0 \le t \le t^r_0 + M^r$ and $h^r_0 \le h \le h^r_0 + Q^r$
       • $0 \le Y^n_{ikt} \le 1$ and $B_{ihtn}, H_{ihtn}, S_{ihtn}, P_{ihtn} \in \mathbb{R}^+$ for $t > t^r_0 + M^r$ and $h > h^r_0 + Q^r$
    Solve the approximate sub-problem **[EVC(PHA(r))]** using CPLEX
    if $(t_0 > |\mathcal{T}|)$ **then**
       | $terminate \leftarrow true$;
    else
       | Fixing the value Y^n_{ikt}, $B_{ihtn}, H_{ihtn}, S_{ihtn}, P_{ihtn}$ for $t < t^r_0$ and $h < h^r_0$;
    end
    $r \leftarrow r + 1$;
end
return $z(Y^r_{ikt})$

Let [**EVC(PHA(r))**] be an approximate sub-problem of the RH algorithm at iteration r. We further let t^r_0, h^r_0, M^r, and Q^r be the starting time period for years, hours, and number of time periods for years and hours for each sub-problem r, respectively. In the RH heuristic, one can either set a fixed value of M^r and Q^r or vary them across different iterations of the algorithm. For each scenario $n \in \mathcal{N}$, the approximate sub-problems [**EVC(PHA(r))**] are solved by setting the variables as:

$$\begin{cases} \{Y^n_{ikt}\} \in \{0, 1\} and \{B_{ihtn}, H_{ihtn}, S_{ihtn}, P_{ihtn}\} \in \mathbb{Z}^+ for t^r_0 \leqslant t \leqslant t^r_0 + M^r and h^r_0 \leqslant h \leqslant h^r_0 + Q^r \\ 0 \leqslant Y^n_{ikt} \leqslant 1 \,\&\, B_{ihtn}, H_{ihtn}, S_{ihtn}, p_{ihtn} \in \mathbb{R}^+ for t > t^r_0 + M^r \,\&\, h > h^r_0 + Q^r \end{cases}$$

After solving a sub-problem, we fix the values of $Y^{n,r}_{ikt} = Y^{n,r-1}_{ikt}$, $\forall i \in \mathcal{I}, k \in \mathcal{K}, t \in \mathcal{T}$; $B^r_{ihtn} = B^{r-1}_{ihtn}$, $\forall i \in \mathcal{I}, h \in \mathcal{H}, t \in \mathcal{T}$; $H^r_{ihtn} = H^{r-1}_{ihtn}$, $\forall i \in \mathcal{I}, h \in \mathcal{H}, t \in \mathcal{T}$; $S^r_{ihtn} = S^{r-1}_{ihtn}$, $\forall i \in \mathcal{I}, h \in \mathcal{H}, t \in \mathcal{T}$; and $P^r_{ihtn} = P^{r-1}_{ihtn}$, $\forall i \in \mathcal{I}$, $h \in \mathcal{H}, t \in \mathcal{T}$ for $t < t^r_0$ and $h < h^r_0$ and step size r is updated. Note that by varying parameters t^r_0, h^r_0, M^r, and Q^r, several different variants of the RH algorithm can be developed. Figs. 2–4 provide an illustration of solving a three-year and four-hour time period problem using three different variants of the RH heuristic (**[RH1]**-**[RH3]**). Through multiple numerical experiments discussed in Section 4.3, we will identify which variant of the RH heuristic solves problem [**EVC(PHA(r))**] efficiently.

4. Computational study and managerial insights

In order to test the performance of the algorithms proposed in Section 3 and to draw managerial insights, we develop a case study where we use Washington, D.C. as a testing ground for the analysis. All the algorithms proposed in this study are coded in GAMS 24.2.1 (General Algebraic Modeling System, 2013) and executed on a desktop computer with an Intel Core i7 3.50 GHz processor and 16.0 GB RAM. The optimization solver used is ILOG CPLEX 12.6.[4] In this section, we first provide the details about the input parameters used to develop the case study. Next, we discuss the results obtained from the experimental study and then present the computational performance of the hybrid Sample Average approximation based Progressive Hedging Algorithm to solve model **[EVC]**.

---

[4] https://www-01.ibm.com/software/commerce/optimization/cplex-optimizer/.
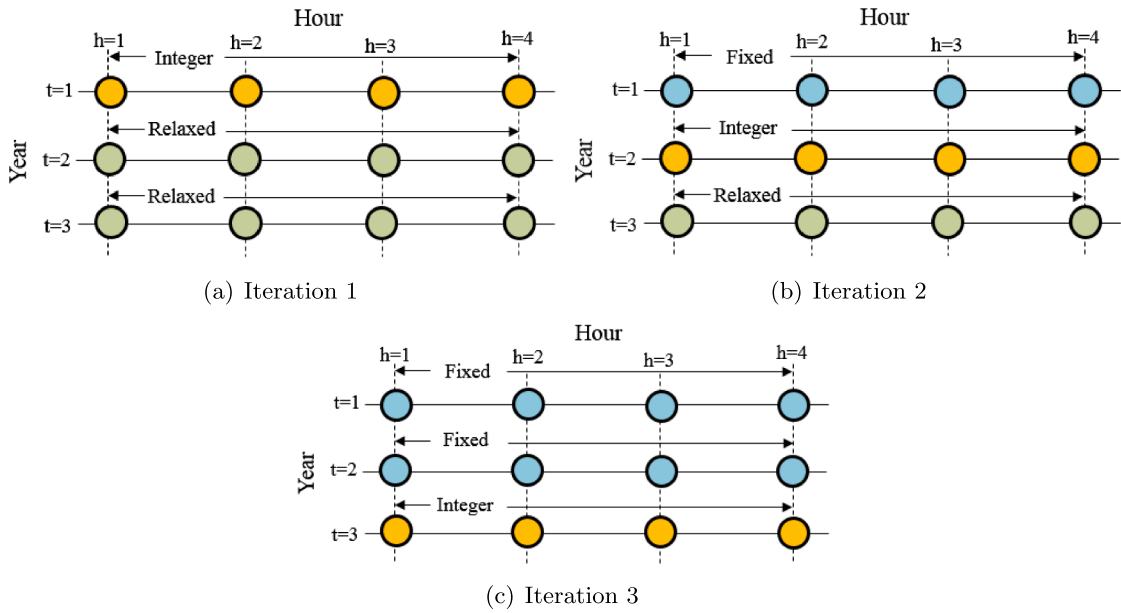
Fig. 2. Illustration of a rolling horizon strategy for **[RH1]**.
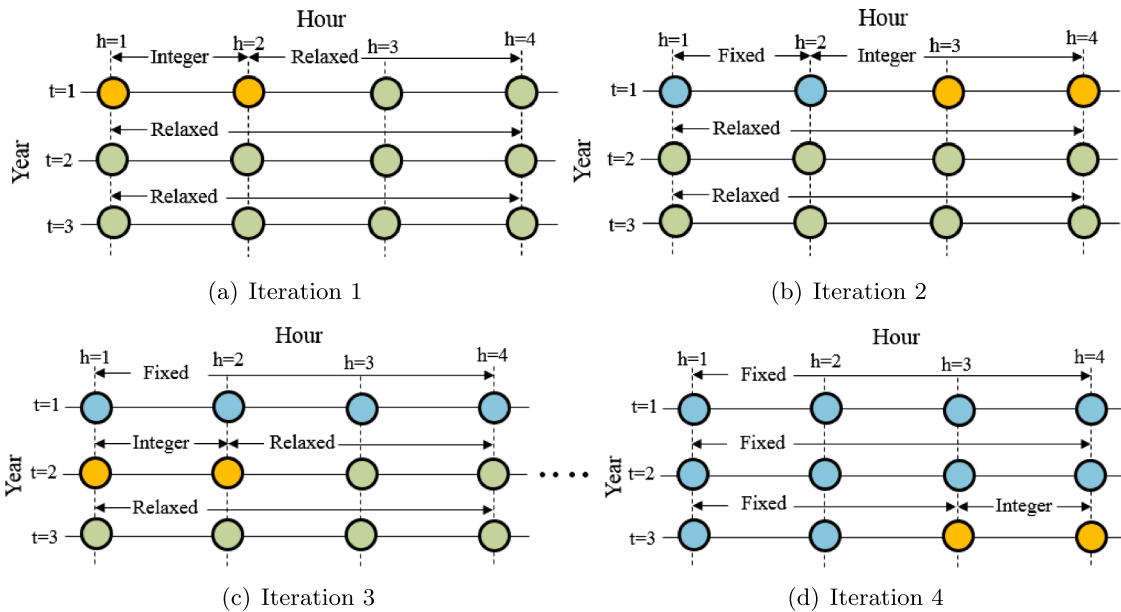
Fig. 3. Illustration of a rolling horizon strategy for **[RH2]**.

4.1. Input parameters

This study considers Washington, D.C. as a testing ground to visualize and validate the modeling results. A network representation along with demand distribution of Washington, D.C. is shown in Fig. 5. The rationale behind selecting Washington, D.C. is that the city offers incentives to own electric vehicle and the adoption rate is high. We divide the network into cells (i. e., $|I| = 132$) where each cell contributes an area of approximately 1.0 mile^2. The data for cell-specific parameters are obtained only for those that have a road passing through them; otherwise, the values for those cells are set to zero. Thus, it is reasonable to assume that only the active cells can be considered for potential location of opening a charging station. We have considered a 5-year planning horizon starting in 2017 and ending in 2021 ($|T| = 5$). Further, we have drawn a representative 24 h from each year of the planning horizon to account for the short term operational decisions ($|H| = 24$). Note that all the cost components are calculated based on 2017 dollars and are adjusted based on inflation. The cost of opening a fast electric vehicle charging station (ψ_{ik_1t}) at cell $i \in I$ costs \$50,000 (Agenbroad and Hollland, 2014) while the cost increases to \$500,000 to open a charging station with battery swap station (ψ_{ik_2t}) (Gigaom, 2015).

(a) Iteration 1   (b) Iteration 2

(c) Iteration 3
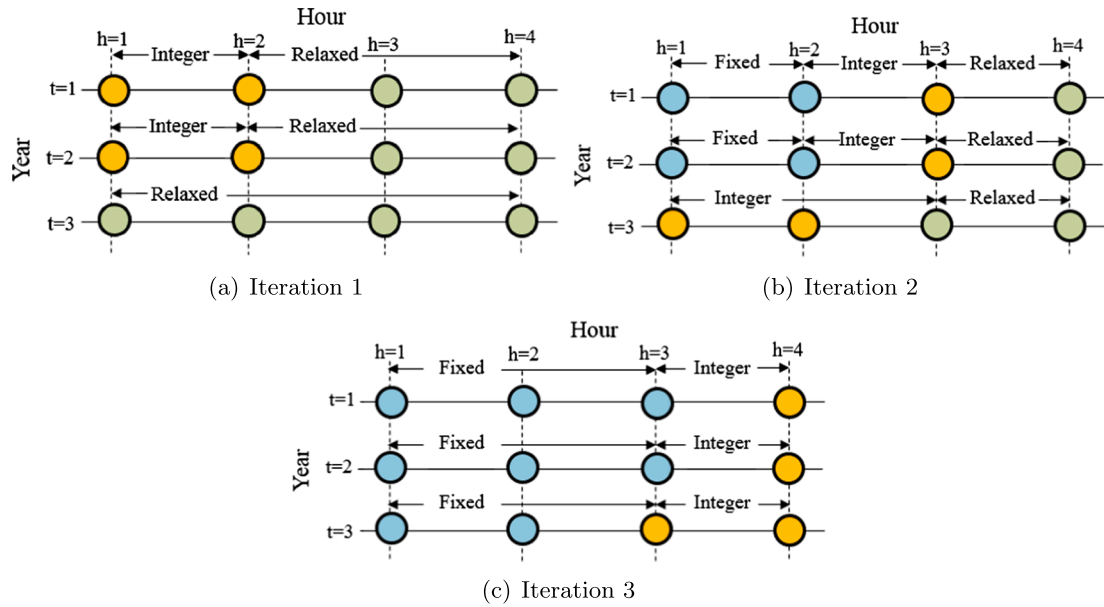
Fig. 4. Illustration of a rolling horizon strategy for **[RH3]**.

(a)   (b)
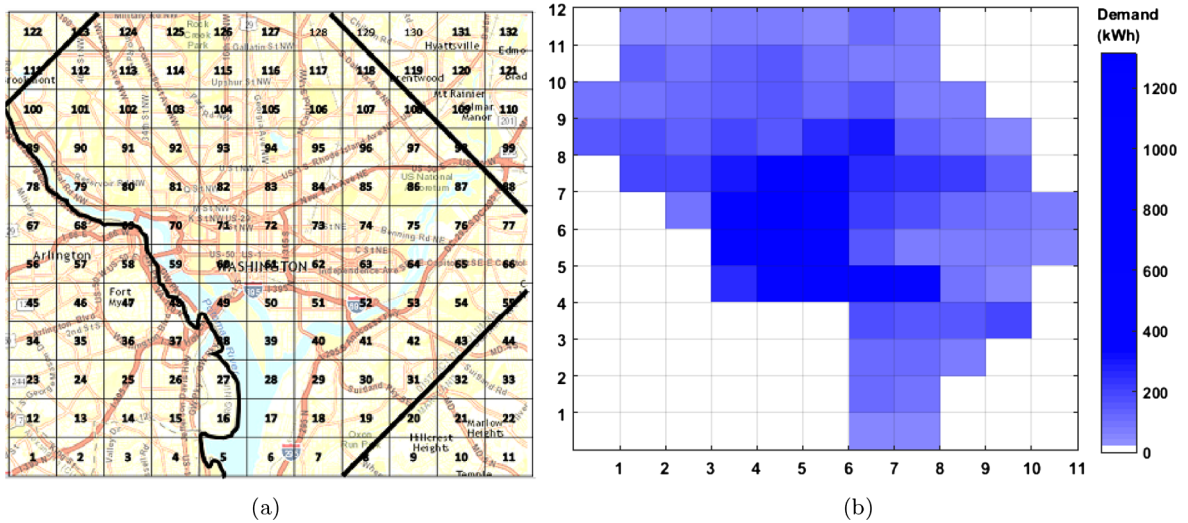
Fig. 5. Network representation (Original map obtained from ArcGIS (2016)) and geographical demand distribution of.Washington, D.C.

Even though the cost of opening a charging station varies from one cell to another; however, in this study we have assumed a fixed investment cost for all the charging stations opened in cell $i \in \mathcal{I}$ for a reasonable approximation. The hourly electricity price plan for PG c_{ht}^{pg}, renewable resources c_{ht}^r, and V2G c_{ht}^{v2g} are obtained from Salt River Project (2015),Solar Cell Central (2016), and Plug in America (2016). We project the flow of cars f_{iht} at each cell $i \in \mathcal{I}$ of hour $h \in \mathcal{H}$ in year $t \in \mathcal{T}$ based on the number of electric vehicles available at Washington, D.C. in 2014. We used the information that there are 8,275 electric vehicles on Washington, D.C. roads (Plug In Sites, 2014). Factors such as density of population, hospitals, and colleges located near major roads are considered to project f_{iht}. It is assumed that electric vehicle flow is increasing annually. Many studies predict that there will be a vast increase in sales of electric vehicles. For instance, Trochaniak (2016) shows how the increase in electric vehicle sales has grown from 2014 to 2016. With another study, Becker et al. (2009) makes predictions on electric vehicle adoption growth rate until 2030. The study shows that there will be an increasing trend in electric vehicle sales compared to hybrid and traditional combustion engine cars. Flow is measured by only considering cells that have a road passing through. The flow is considered cumulative, in the sense that if the road forks demand is divided between the separating roads and if two roads join, then the demand is accumulated. Based on the number of electric vehicles in 2014, we assumed a different electric vehicle adoption growth rate for the yearly increase in demand. Since this information cannot be obtained in advance due to its stochastic nature, we regarded charging stations' demand as an uncertain parameter in the study. Demand for each charging station is obtained by multiplying the number of cars flowing f_{iht} by the

Table 2
Summary of input data.

Parameters	Symbol	Value	References
Fixed cost of opening charging station of type I	ψ_{ik_1t}	$50,000	Agenbroad and Hollland (2014)
Fixed cost of opening charging station of type II	ψ_{ik_2t}	$500,000	Gigaom (2015)
Unit PG electricity price	c_{ht}^{pg}	$(0.06–0.15)/kWh	Salt River Project (2015)
Unit cost of producing electricity from renewable resources	c_{ht}^{r}	$0.099/kWh	Solar Cell Central (2016)
Unit V2G electricity price	c_{ht}^{v2g}	$(0.05–0.13)/kWh	Plug in America (2016)
Flow of electric vehicles	f_{iht}	8275/day	Plug In Sites (2014)
Car charging percentage	$\eta_{ht\omega}$	40%	Assumed
Car discharging percentage	β_{ht}	5%	Assumed
Cost of storing a battery	δ_{ht}	$0.02/hr	Assumed
Average unit power requirement for each car	λ	35.6 kWh/car	Assumed
Average power discharged from each car	γ	35.6 kWh/car	Assumed

average electric vehicle charge requirement λ and the percentage of flow requesting a charge $\eta_{ht\omega}$. We set the car charging percentage $\eta_{ht\omega} = 40\%$ and the car discharging percentage $\beta_{ht} = 5\%$ in our base case experiments. The availability of grid power g_{iht} and renewable resources r_{iht} are adopted from the Energy Information Administration (2016) and Public Service Public Service Commission of the District of Columbia (2016), respectively. The cost of storing a battery in a *Type 2* charging station is set to be $\delta_{ht} = $ "$"0.02/hr. Finally, we set average unit power requirement for each car λ to be 35.6 kWh and average unit power discharged from each car γ to be 35.6 kWh, respectively, in our base case experimentations. Table 2 provides a summary of the input data used in the model.

4.2. Experimental results

A sensitivity analysis is performed to determine how different values of an independent parameter impact a particular dependent variable(s) as well as the overall electricity supply network cost and design, under a given set of assumptions. Annual decisions on established charging stations determine the electricity supply network design. Therefore, a considerable change in critical factors

(a) Year 2017 (b) Year 2018 (c) Year 2019

(d) Year 2020 (e) Year 2021
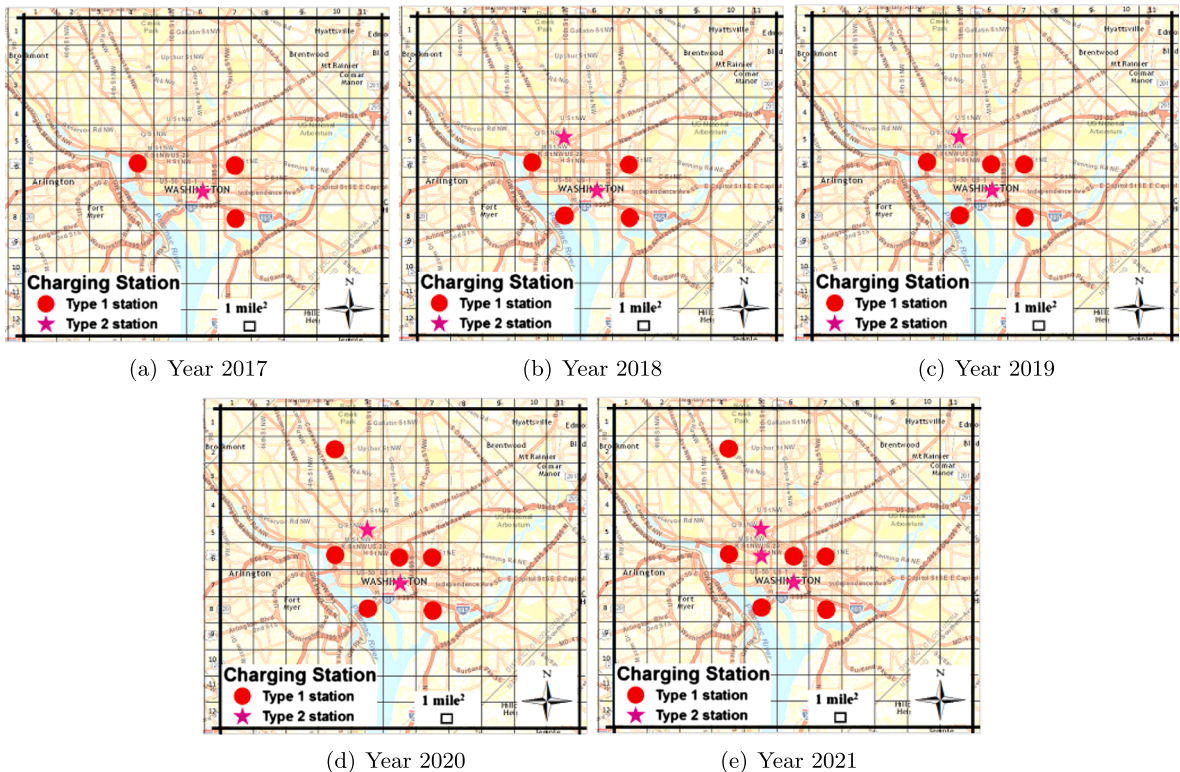
Fig. 6. Electric vehicle charging station location under base case scenario.

results in changes in network design. The impact of the car charging percentage, available energy resources (e.g., PG, renewable, and V2G), minimum power requirement to establish a charging station, and solar power utilization on the overall electricity supply network design and cost are analyzed.

All sensitivity analyses are performed with respect to a real life case study developed for Washington, D.C. (base case study). Fig. 6 shows the deployment of charging stations $\mathbf{Y}$ (symbol "•" represents *type 1* charging station and "★" represents *type 2* charging station) for the base case experimentation. Results indicate that the model **[EVC]** decides to open a number of charging stations near the downtown area of Washington, D.C. since the density flow of electric vehicles to those cells are high. We further observe a noticeable expansion of charging stations in Washington, D.C. from year 2017–2021.

In the following, the impact of critical parameters on the electricity supply network cost and design are determined. We denote $\overline{G}_{iht\omega} = \sum_{i\in\mathcal{I},h\in\mathcal{H},t\in\mathcal{T},\omega\in\Omega} \rho_\omega G_{iht\omega}/|\mathbf{Y}_t|$ to be the average consumption of grid in a charging station located in cell $i \in \mathcal{I}$ on hour $h \in \mathcal{H}$ of year $t \in \mathcal{T}$. Moreover, $|\mathbf{Y}_t|$ is considered as the number of charging stations of any type established at the electricity supply network in a particular year t. Likewise, we denote $\overline{Z}_{iht\omega}, \overline{V}_{iht\omega}$, are representatives of an average of hourly electricity power supplied by solar power and V2G power, respectively, related to any type of charging stations established at any network cell. In addition, $\overline{B}_{iht\omega} = \sum_{i\in\mathcal{I},h\in\mathcal{H},t\in\mathcal{T},\omega\in\Omega} \rho_\omega B_{iht\omega}/|\mathbf{Y}_t'|$ is considered as a representative of the average number of batteries, which are hourly utilized at a type 2 charging station established at any network cell. Similarly, $\overline{H}_{iht\omega}, \overline{S}_{iht\omega}$, and $\overline{P}_{iht\omega}$ are considered as representatives of the average number of batteries, which are hourly stored, charged, and discharged at a type 2 charging station established at any network cell, respectively. In addition, $|\mathbf{Y}_t'|$ is considered as the number of type 2 charging stations established at the electricity supply network in a particular year t.

4.2.1. Impact of car charging percentage ($\eta_{ht\omega}$) variability on system performance

The next set of experiments show how different levels of car charging percentage variations $\eta_{ht\omega}$ impact the system performance. To achieve this goal, we created three different realistic scenarios. In the first scenario (base case), we solve model **[EVC]** using the input parameters discussed in Section 4.1. The second and third scenarios are created by setting $\epsilon = 50\%$ and $\epsilon = 5\%$ to represent *high* and *low* car charging percentage variation levels. Note that we employ the Monte Carlo simulation to generate different car charging percentage scenarios $\eta_{ht\omega}$ within $[\overline{\eta}_{ht}(1-\epsilon), \overline{\eta}_{ht}(1+\epsilon)]$ where $\overline{\eta}_{ht}$ represents the mean car charging percentage scenario for each hour $h \in \mathcal{H}$ in year $t \in \mathcal{T}$.

Fig. 7 demonstrates the impact of car charging percentage variability $\eta_{ht\omega}$ on system performance. As evidenced from the results, as the level of car charging percentage variability $\eta_{ht\omega}$ increases, the amount of power utilized to satisfy the electricity demand from diversified power sources (*e. g*., grid, solar, V2G) also increases. Clearly, model **[EVC]** is highly responsive to a number of time-dependent parameters such as solar power availability, electricity prices, and vehicle flows, which severely impact the hourly operational decisions of a charging station located in cell $i \in \mathcal{I}$ of a given year $t \in \mathcal{T}$. For instance, it is observed that the electric vehicle power demand is satisfied primarily via grid and V2G during low cost operating hours and solar power unavailability (*i. e*., from 8:0 P.M. to 8:0 A.M.). Alternatively, the demand is satisfied first via solar and then via grid and V2G during peak operating hours (*i. e*., from 10:0 A.M. to 2:0 P.M.) and solar power availability. Fig. 8 demonstrates the impact of car charging percentage variability $\eta_{ht\omega}$ on the battery-related decisions when model **[EVC]** decides to open *type 2* charging stations in our tested region. It is observed that to cope with high power demand variability $\eta_{ht\omega}$, the charging stations decide to charge more batteries during off peak hours (shown in Fig. 8(c)) which they discharge during peak hours (shown in Fig. 8(d)). As more batteries are charged during off peak hours, more batteries are required to be stored in the charging stations during those operating hours as illustrated in Fig. 8(b). In summary, we observe that the car charging percentage variability $\eta_{ht\omega}$ highly impacts the operational decisions in the electric vehicle charging stations.

4.2.2. Impact of g_{iht}, r_{iht}, and β_{ht} on System Performance

Our proposed model **[EVC]** is highly sensitive to a number of input parameters such as availability of grid power g_{iht}, solar power r_{iht}, and V2G power (V2G power availability depends on car discharging percentage β_{ht}). Changes in power availability may lead to deviations from the desired operation quality and therefore must be quantified and carefully evaluated. To see the impact of these three power availabilities (*e. g*., grid, solar, and V2G) on system performance, we conduct four sets of experiments by varying their availability by $\pm 25\%$ and $\pm 50\%$ from the base case scenario as illustrated in Figs. 9–11. Let us first quantify the performance of grid power availability g_{iht} on system performance (shown in Fig. 9). We keep the solar power r_{iht} and V2G power availability at their base values. We observe that, as the grid power availability g_{iht} decreases by 50%, model **[EVC]** opens 52.94% additional charging stations to meet the electric vehicles power demand (shown Fig. 9(a)). Moreover, by increasing the grid power availability, the average utilization of grid power $\overline{G}_{iht}^\omega$ in a charging station also increases as illustrated in Fig. 9(b).

We now evaluate the system performance by varying solar power availability r_{iht} by $\pm 25\%$ and $\pm 50\%$ from the base case scenario. It is observed that model **[EVC]** decides to open an additional 23.53% charging stations when the solar power availability r_{iht} drops by 50% from the base case scenario. Even though the unavailability of grid and solar power significantly impact the system performance, solar power is relatively less sensitive compared to grid power unavailability. Further, Fig. 10(b) shows that model **[EVC]** increases the average utilization of solar power $\overline{Z}_{iht}^\omega$ in a charging station as soon as the source becomes available. Finally, we investigate the performance of V2G power availability on system performance (shown in Fig. 11). Results indicate that for a 50% decrease in β_{ht} value, model **[EVC]** opens an additional 14.70% charging stations in our tested region (shown in Fig. 11(a)). Clearly, if less cars decide to discharge power in a charging station which is considered as the main source of V2G energy, the system will be relatively less impacted compared to grid and solar power unavailability. This is because grid, followed by solar, are the main sources of energy for the charging stations and their unavailability are expected to impact the system severely as compared to V2G energy.

(a) $\overline{G}_{iht}^{\omega}$ vs. time (hours in years)

(b) $\overline{Z}_{iht}^{\omega}$ vs. time (hours in years)

(c) $\overline{V}_{iht}^{\omega}$ vs. time (hours in years)
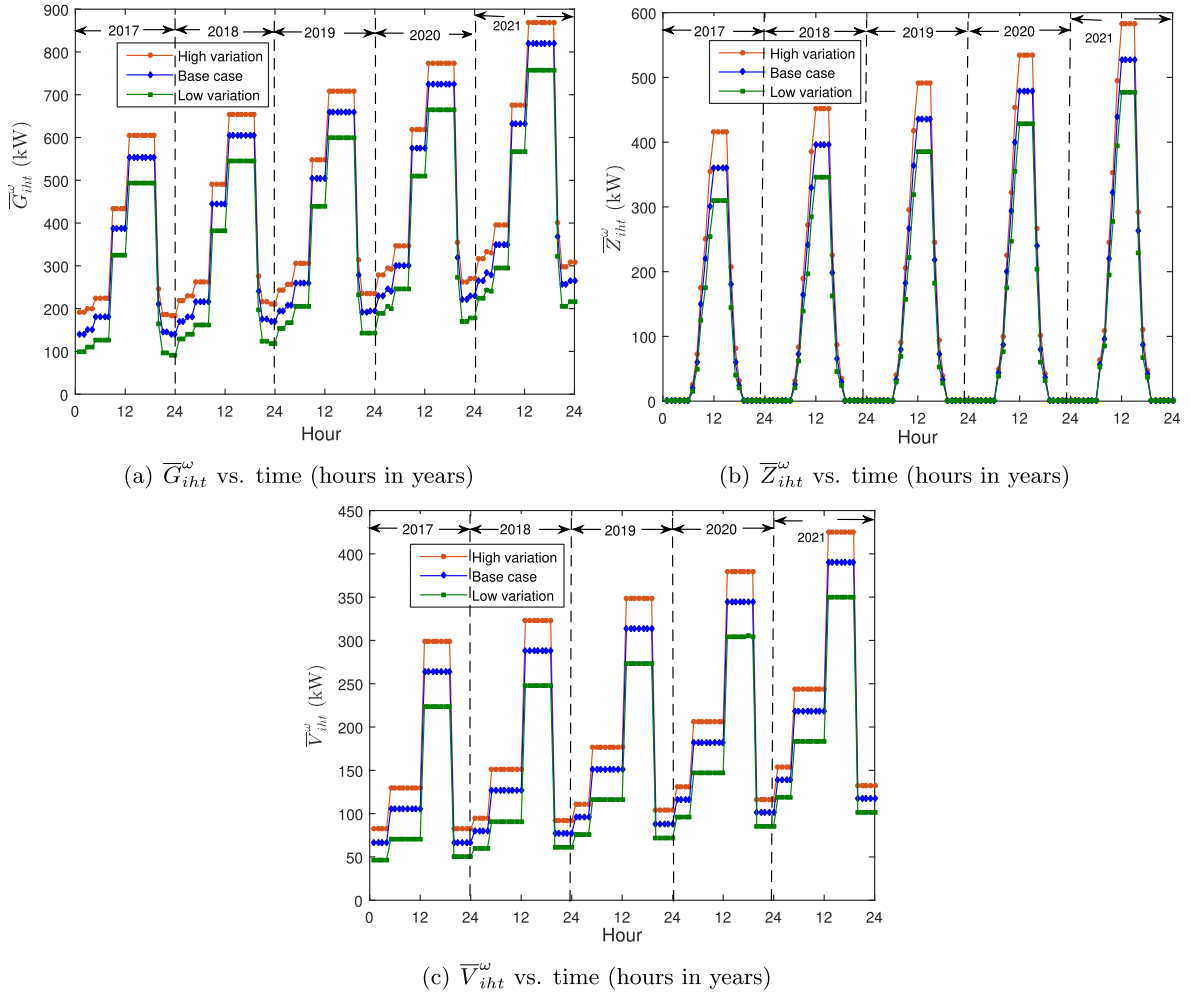
Fig. 7. Impact of car charging percentage (η_t^{ω}) variability on utilizing resources.

We further observe that as the V2G power availability increases, the average utilization of V2G power $\overline{V}_{iht}^{\omega}$ in a charging station located at cell $i \in \mathcal{I}$ in hour $h \in \mathcal{H}$ of year $t \in \mathcal{T}$ also increases (shown in Fig. 11(b)). In summary, we observe that the availability of grid, solar, and V2G energy significantly impacts the long-term charging station location decisions and short-term day-to-day operational decisions (e.g., hourly resource utilization, battery storage decisions).

4.2.3. Impact of p_t^s and p_t^b on system performance

We now analyze the impact of minimum power demand requirements (i.e., p_t^s and p_t^b) to open a charging station on system performance. Fig. 12 illustrates the relationship between charging station opening decisions Y_{ikt} under different p_t^s and p_t^b values. It is obvious from the results that decreasing both p_t^s and p_t^b from the base values increase the opening of both *type 1* and *type 2* charging stations and vice versa. For instance, a 50% decrease in minimum power demand requirement p_t^s increases the average number of charging station opening decisions by 22.2%. A network representation for this scenario is depicted in Fig. 13. However, we observe that changing p_t^b provides less sensitive decisions in opening charging stations compared to p_t^s. For instance, a 50% decrease in minimum power demand requirement p_t^b results in an increase in average number of charging station opening decisions by 10.9%. A network representation for this scenario is depicted in Fig. 14. It is interesting to note that a 50% decrease in p_t^s causes opening a significant number of *type 1* charging stations in a widespread distribution on our tested region as illustrated in Fig. 13. On the other hand, a 50% decrease in p_t^b, though it opens more charging stations, shows less sensitive in opening *type 2* charging stations (as shown in Fig. 14) compared to the base case scenario (shown in Fig. 6).

4.3. Analyzing the performance of solution algorithms

This section presents our computational experience in solving model [**EVC**] using the algorithms proposed in Section 3. We first assess the computational performance of using different variants of the rolling horizon heuristic over CPLEX (shown in Table 4). Next,

(a) $\overline{B}_{iht}^{\omega}$ vs. time (hours in years)

(b) $\overline{H}_{iht}^{\omega}$ vs. time (hours in years)

(c) $\overline{S}_{iht}^{\omega}$ vs. time (hours in years)

(d) $\overline{P}_{iht}^{\omega}$ vs. time (hours in years)
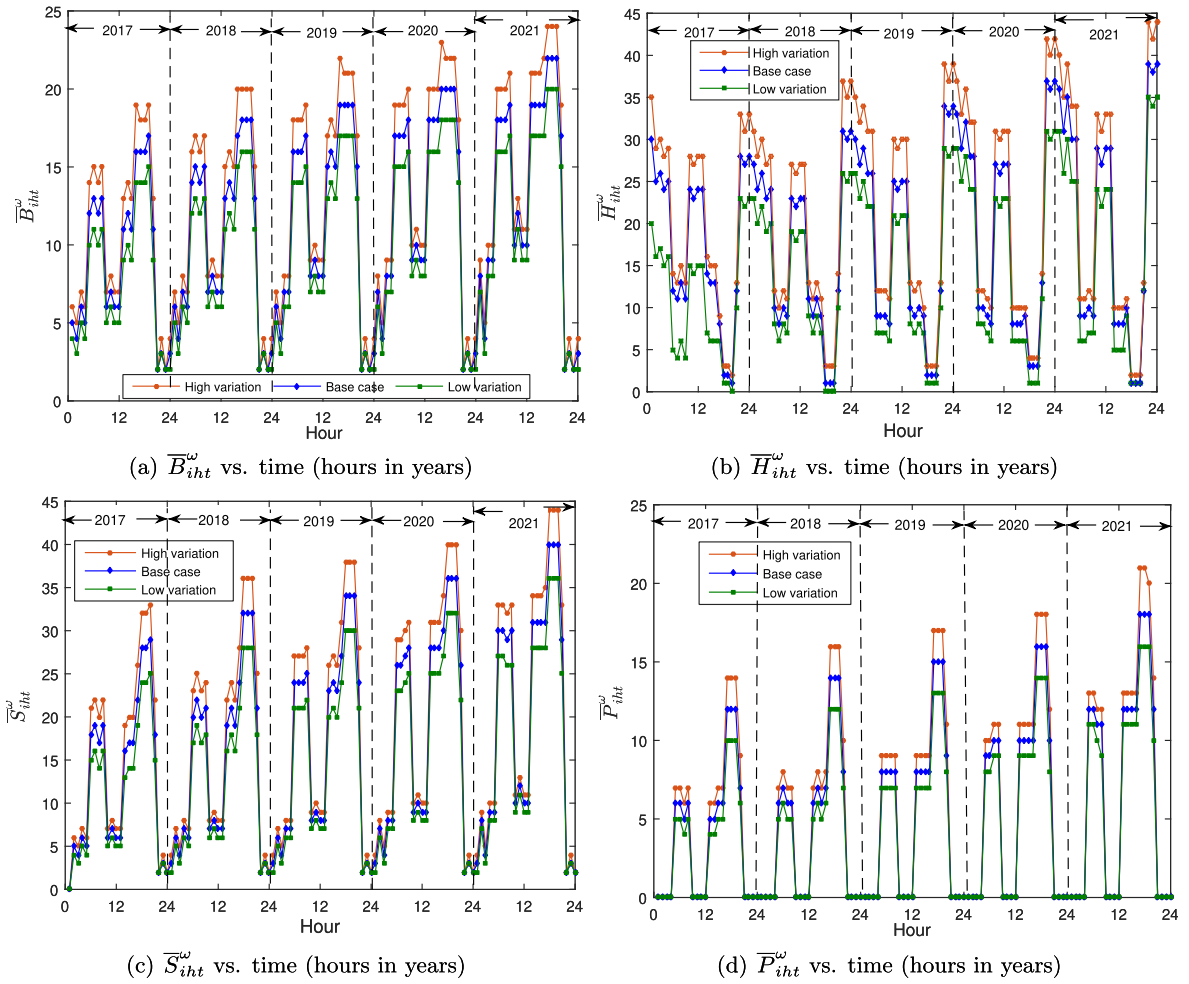
Fig. 8. Impact of car charging percentage (η_t^{ω}) variability on real-time demand response.

(a)

(b)
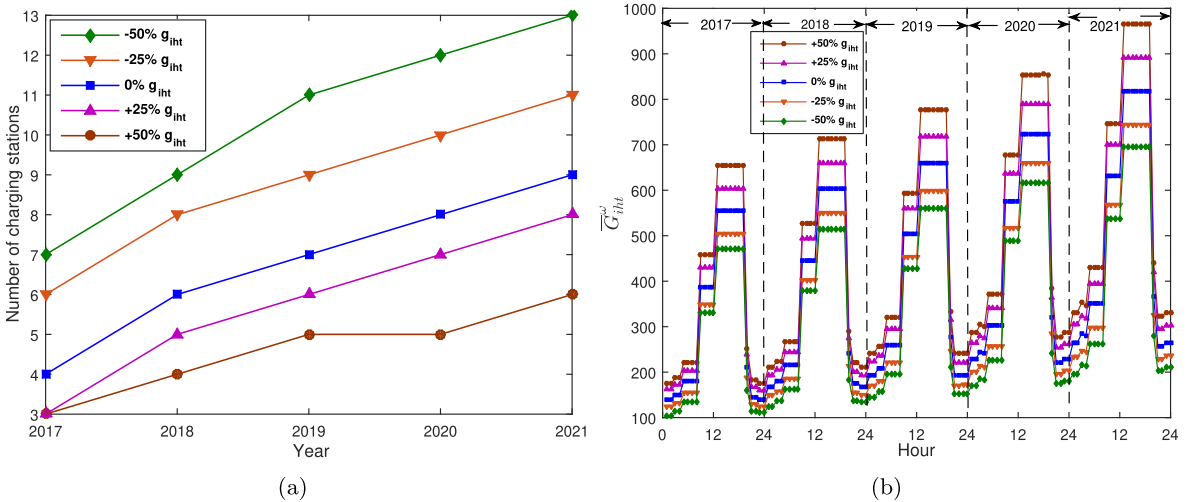
Fig. 9. Impact of PG availability (g_{iht}) on system performance.

(a)   (b)
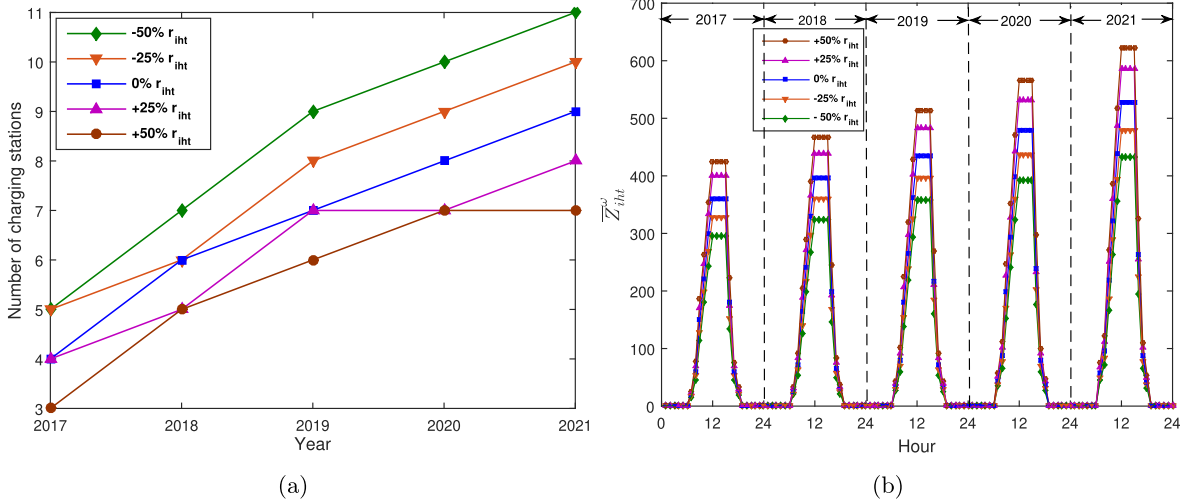
Fig. 10. Impact of solar power availability (r_{iht}) on system performance.

(a)   (b)
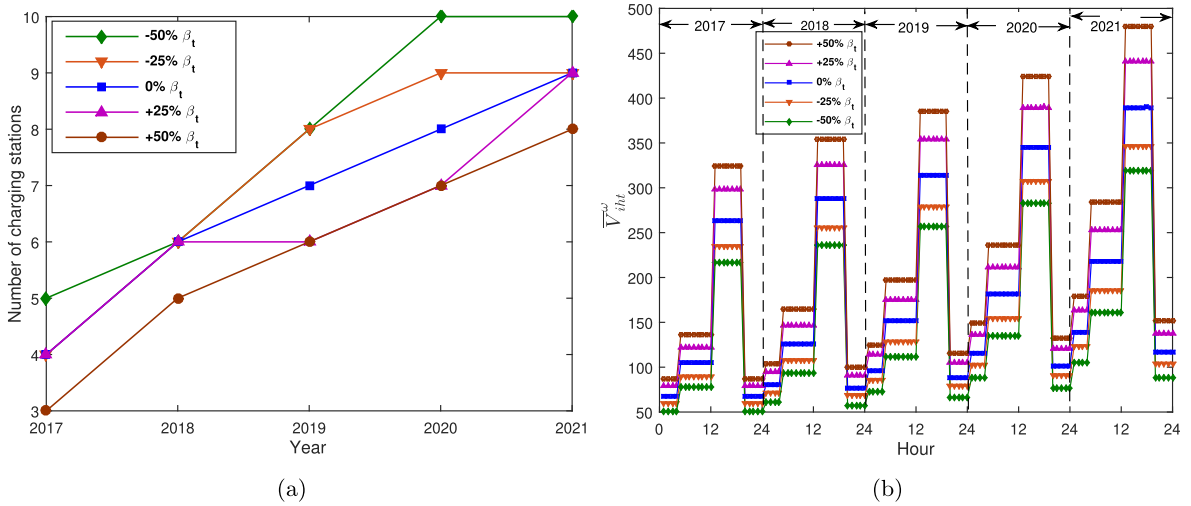
Fig. 11. Impact of V2G power availability (β_t) on system performance.

(a)   (b)
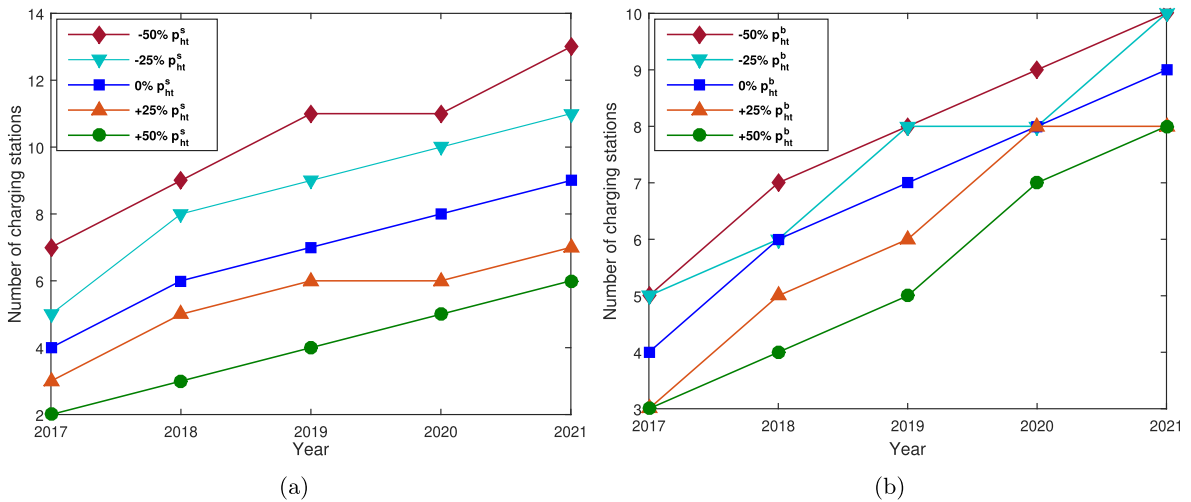
Fig. 12. Impact of p_t^s and p_t^b on system performance.
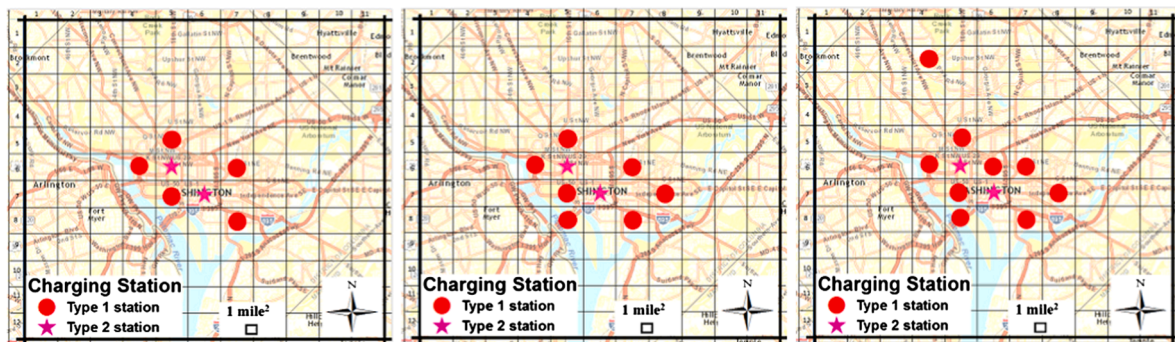
(a) Year 2017   (b) Year 2018   (c) Year 2019
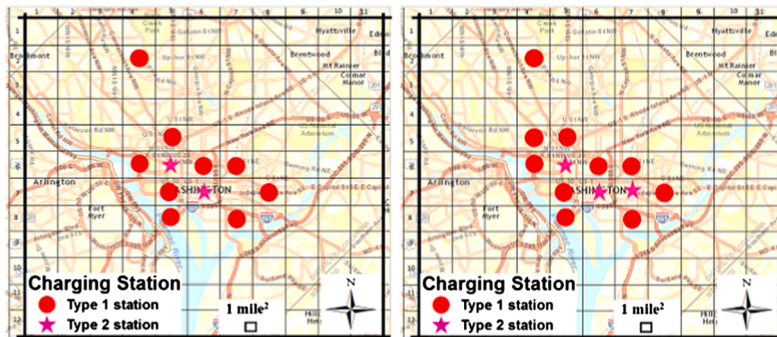
(d) Year 2020   (e) Year 2021

Fig. 13. Electric vehicle charging station location under 50% decrease of p_t^s.
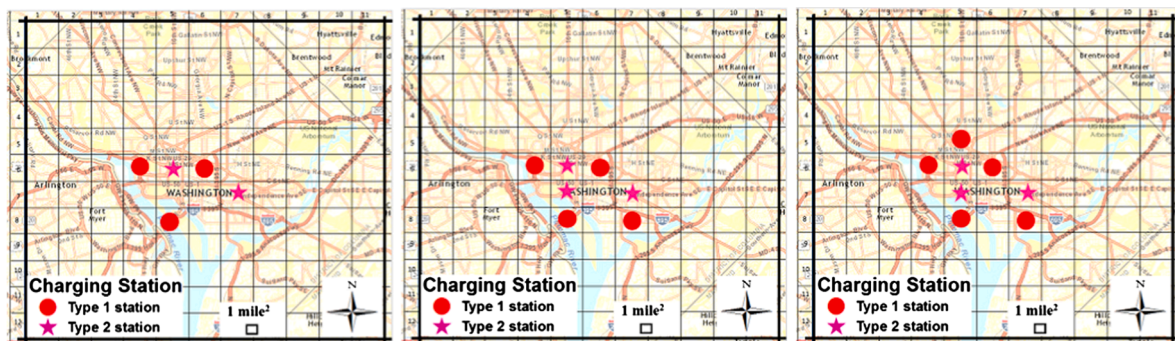
(a) Year 2017   (b) Year 2018   (c) Year 2019
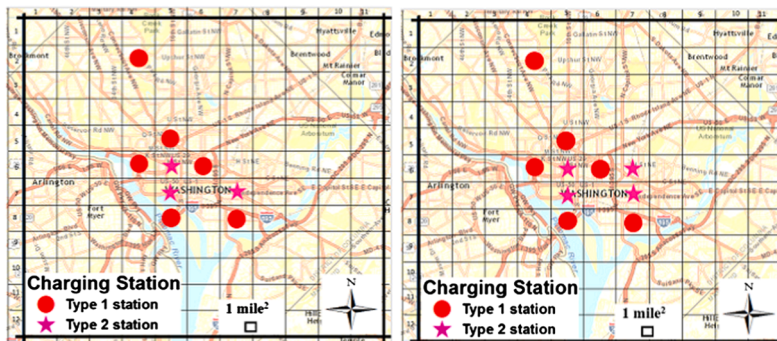
(d) Year 2020   (e) Year 2021

Fig. 14. Electric vehicle charging station location under 50% decrease of p_t^b.

Table 3
Problem size of the test instances.

Case	$|\mathcal{I}|$	$|\mathcal{K}|$	$|\mathcal{H}|$	$|\mathcal{T}|$	Binary Variables	Integer Variables	Continuous Variables	Total Variables	No. of Constraints
1	25	2	12	5	250	6000	6000	12,250	16,370
2	25	2	12	10	500	12,000	12,000	24,500	32,740
3	25	2	24	5	250	12,000	12,000	24,250	31,490
4	25	2	24	10	500	24,000	24,000	48,500	62,980
5	25	2	48	5	250	24,000	24,000	48,250	61,730
6	25	2	48	10	500	48,000	48,000	96,500	123,460
7	50	2	12	5	500	12,000	12,000	24,500	32,620
8	50	2	12	10	1000	24,000	24,000	49,000	65,240
9	50	2	24	5	500	24,000	24,000	48,500	62,740
10	50	2	24	10	1000	48,000	48,000	97,000	125,480
11	50	2	48	5	500	48,000	48,000	96,500	122,980
12	50	2	48	10	1000	96,000	96,000	193,000	245,960
13	100	2	12	5	1000	24,000	24,000	49,000	65,120
14	100	2	12	10	2000	48,000	48,000	98,000	130,240
15	100	2	24	5	1000	48,000	48,000	97,000	125,480
16	100	2	24	10	2000	96,000	96,000	194,000	250,480
17	100	2	48	5	1000	96,000	96,000	193,000	245,480
18	100	2	48	10	2000	96,000	96,000	194,000	250,480
19	132	2	12	5	1320	31,680	31,680	64,680	85,920
20	132	2	12	10	2640	63,360	63,360	129,360	171,840
21	132	2	24	5	1320	63,360	63,360	128,040	165,240
22	132	2	24	10	2640	126,720	126,720	256,080	330,480
23	132	2	48	5	1320	126,720	126,720	254,760	323,880
24	132	2	48	10	2640	253,440	253,440	509,520	647,760

we show how different heuristic strategies enhance the performance of the Progressive Hedging Algorithm (shown in Table 5). Finally, we compare the computational performance of incorporating different accelerated techniques inside the Sample Average Approximation algorithmic framework (shown in Table 6). To help the readers follow our solution methods, we have used the following notations to represent the algorithms:

- **[SAA]**: Sample Average Approximation (SAA) algorithm (described in Section 3)
- **[PHA]**: Progressive Hedging Algorithm (PHA) (described in Section 3)
- **[Hybrid-1]**: Sample average approximation algorithm where the subproblems of the **[SAA]** are solved using the Progressive Hedging Algorithm (PHA) (described in Section 3)
- **[Hybrid-2]**: Sample average approximation algorithm where the subproblems of the **[SAA]** are solved using an enhanced Progressive Hedging Algorithm (PHA) (enhancement techniques are described in Sections 3.3.1 and 3.3.2)
- **[Hybrid-3]**: Sample average approximation algorithm where the subproblems of the **[SAA]** are solved using an enhanced Progressive Hedging Algorithm (PHA) (enhancement techniques are described in Sections 3.3.1, 3.3.2, and

The algorithms presented above are terminated when at least one of the following criteria is met: (a) the optimality gap (*i. e.*, $\epsilon = |UB - LB|/UB$) falls below a threshold value of $\epsilon = 0.01$, or (b) the maximum time limit $time^{max} = 36,000$ (in CPU seconds), or (c) the maximum number of iterations $iter^{max} = 100$ is reached. To terminate the Progressive Heading Algorithm, we have used additional stopping criteria which are described at the end of Section 3.2. The columns of the tables presented in this section provide the optimality gap (represented by *GAP*), running time of the algorithms (represented by *CPU*), and the corresponding number of iterations (represented by *Iter*). In the experimental results, if the algorithms are solved less than the stopping criteria (ϵ) then we highlight the approach which gives the smallest running time. Otherwise, if such a quality solution is not found within the maximum time or iteration limit, then the approach with the smallest optimality gap is highlighted. The size of the deterministic equivalent problem of model [**EVC**] is presented in Table 3.

The first set of experiments (reported in Table 4) present the computational performance in solving model [**EVC**] using three variants of the rolling horizon heuristic (*e. g.*, algorithm [**RH1**], [**RH2**], and [**RH3**]) over CPLEX. To test the performance of these algorithms, we vary $|\mathcal{I}|$, $|\mathcal{H}|$, and $|\mathcal{T}|$ to obtain 18 different problem instances as reported in Table 3. Note that each subproblem of the rolling horizon heuristic is solved using CPLEX, and we set a maximum time limit of 10,800 CPU seconds for each of the subproblems. It is worth noting that the bold values indicate the respective algorithm provides the best solution in Tables 4–6. Results indicate that CPLEX offers high-quality solutions over different variants of the rolling horizon heuristic when the problem size is fairly small (*e. g.*, *Cases 1 to 3*). However, the true benefits of using different variants of the rolling horizon heuristic over CPLEX become more apparent when the problem size increases as can be observed from the results in Table 4. For instance, it is observed from the results that when the problem size increases (i.e., $|\mathcal{I}| > 100$), CPLEX is unable to solve the Washington, D.C. network problem by obeying pre-specified termination criteria. Further, we observe that algorithm [**RH3**], on average, provides 21.7% and 35.3% faster solutions than algorithms [**RH1**] and [**RH2**], respectively. Note that, on average, algorithm [**RH3**] not only provides a competitive running time but also

Table 4
Comparison between different variants of the rolling horizon heuristic over CPLEX

Case	[CPLEX]		[RH1]		[RH2]		[RH3]	
	GAP (%)	CPU (sec)	GAP (%)	CPU (sec)	GAP (%)	CPU (sec)	GAP (%)	CPU (sec)
1	0.38	**283.6**	0.89	335.9	0.74	434.2	0.85	296.8
2	0.46	**414.3**	0.68	587.8	0.81	576.5	0.59	438.6
3	0.77	**387.9**	0.64	493.2	0.57	460.2	0.76	563.3
4	0.96	1283.4	0.79	**774.6**	0.91	1065.4	0.74	797.6
5	0.75	1158.3	0.71	798.3	0.86	736.5	0.88	**682.4**
6	0.49	15,124.6	0.81	8106.5	0.92	8956.4	0.78	**6023.5**
7	0.82	**413.5**	0.79	489.5	0.69	653.8	0.83	427.4
8	0.46	1558.3	0.63	825.7	0.86	1089.6	0.77	**863.3**
9	0.68	1247.8	0.89	841.5	0.97	895.2	0.79	**724.2**
10	0.98	16,650.6	0.66	9842.7	0.87	10,454.8	0.63	**7496.6**
11	0.36	15,247.3	0.76	8256.4	0.84	9182.1	0.75	**6161.8**
12	3.15	36,000	0.84	9914.2	0.92	10,189.6	0.63	**8225.7**
13	0.84	1584.6	0.71	889.3	0.85	1083.6	0.75	**851.1**
14	0.74	17,524.8	0.87	10,378.3	0.87	11,621.2	0.86	**9223.5**
15	0.89	16,632.8	0.98	9963.7	0.79	10,503.9	0.69	**7563.8**
16	8.68	36,000	3.41[a]	14,425.4	4.81[a]	16,123.5	1. 82[a]	12,463.2
17	4.32	36,000	2.87[a]	11,351.6	2.68[a]	14,869.4	1. 06[a]	10,982.7
18	15.63	36,000	4.15[a]	18,362.6	3.41[a]	19,658.8	2. 89[a]	13,864.2
Average	2.30	12,972.8	1.23	5924.3	1.30	6586.4	0.95	**4869.4**

[a] Unable to solve the first subproblem within 10,800 CPU seconds.

Table 5
Performance of different variant of the rolling horizon heuristic in **[PHA]**

Case	[PHA + HR + RH1]		[PHA + HR + RH2]		[PHA + HR + RH3]	
	GAP (%)	CPU (sec)	GAP (%)	CPU (sec)	GAP (%)	CPU (sec)
1	0.67	**70.9**	0.74	84.2	0.79	76.8
2	0.58	**124.8**	0.67	167.4	0.68	138.6
3	0.74	143.2	0.72	180.2	0.46	**113.5**
4	0.79	424.6	0.81	565.4	0.68	**397.4**
5	0.84	468.3	0.87	586.1	0.81	**422.4**
6	0.87	4523.1	0.81	5524.4	0.75	**3024.6**
7	0.64	139.3	0.57	173.8	0.33	**127.1**
8	0.79	525.7	0.76	689.1	0.64	**463.3**
9	0.84	541.2	0.85	675.7	0.72	**424.2**
10	0.75	4682.1	0.67	5682.6	0.64	**3424.1**
11	0.82	4782.1	0.91	5482.8	0.88	**3661.8**
12	0.78	6784.1	0.91	7425.3	0.71	**4965.3**
13	0.76	519.5	0.78	784.4	0.81	**454.2**
14	0.78	4876.4	0.87	5687.3	0.78	**3854.1**
15	0.81	4613.4	0.84	5541.1	0.87	**3546.4**
16	0.84	9414.1	0.75	10,243.5	0.87	**6786.5**
17	0.91	8756.7	0.97	9874.6	0.84	**6014.7**
18	14.15	36,000	18.41	36,000	**2.89**	36,000
Average	1.52	4854.9	1.77	5298.2	0.84	**4105.3**

offers high-quality solution over algorithms [**RH1**] and [**RH2**], respectively. In summary, algorithm [**RH3**] seems to offer high-quality solutions consistently within the experimental range.

The second set of experiments analyzes how different variants of the rolling horizon heuristic enhance the performance of the Progressive Hedging Algorithm (shown in Table 5). We employ the following enhancement techniques: (*i*)[**PHA + HR + RH1**] that incorporates the first variant of the rolling horizon heuristic [**RH1**];(*ii*)[**PHA + HR + RH2**] that incorporates the second variant of the rolling horizon heuristic [**RH2**]; and (*iii*)[**PHA + HR + RH3**] that incorporates the third variant of the rolling horizon heuristic [**RH3**] inside the [**PHA**] algorithm. Note that in all the enhancement techniques discussed in (*i*) − (*iii*), we incorporate the penalty parameter updating techniques (described in Section 3.3.1) and heuristic strategies (described in Section 3.3.2) inside the [**PHA**] algorithmic framework. We test the performance of the algorithms by fixing the scenario size $N = 50$ while varying $|\mathcal{I}|$, $|\mathcal{H}|$, and $|\mathcal{T}|$ to obtain 18 different problem instances as reported in Table 3. It is observed from Table 5 that algorithm [**PHA + HR + RH3**]

Table 6
Comparison of different solution algorithms.

Case	N	M	[SAA] GAP (%)	CPU (sec)	Iter	[Hybrid-1] GAP (%)	CPU (sec)	Iter	[Hybrid-2] GAP (%)	CPU (sec)	Iter	[Hybrid-3] GAP (%)	CPU (sec)	Iter
19	20	5	0.79	2532.3	1	0.64	1732.5	2	0.77	932.7	2	0.33	**632.3**	1
		10	0.81	2712.4	1	0.64	1934.5	1	0.59	1025.8	2	0.47	**724.6**	1
	40	5	0.62	6814.5	1	0.79	2042.4	1	0.76	1186.2	1	0.44	**816.3**	2
		10	0.74	9552.4	1	0.87	3684.4	2	0.76	1632.4	1	0.63	**1153.6**	1
20	20	5	3.41	36,000	1	0.74	4056.5	1	0.84	2423.5	1	0.58	**1363.7**	1
		10	4.52	36,000	1	0.78	4634.8	1	0.97	2687.6	2	0.71	**1463.5**	2
	40	5	5.69	36,000	1	0.81	5563.6	2	0.78	3125.7	1	0.65	**1623.4**	1
		10	12.69	36,000	1	0.76	7563.6	2	0.87	4225.7	1	0.55	**1896.3**	1
21	20	5	10.36	36,000	1	4.32	36,000	1	0.85	6475.6	1	0.84	**2954.2**	1
		10	15.36	36,000	1	6.54	36,000	2	0.69	7635.7	1	0.54	**3654.3**	1
	40	5	11.35	36,000	1	5.5	36,000	1	0.85	8656.3	1	0.48	**4157.6**	2
		10	*mem*[a]	–	-	6.63	36,000	2	0.67	9542.8	2	0.59	**4598.4**	1
22	20	5	*mem*	–	–	5.62	36,000	1	0.82	10,563.4	1	0.23	**4624.5**	1
		10	*mem*	–	–	8.63	36,000	1	0.71	11,123.3	1	0.51	**4869.2**	1
	40	5	*mem*	–	–	6.52	36,000	1	0.87	12,415.3	1	0.74	**5168.3**	1
		10	*mem*	–	–	9.41	36,000	2	0.84	14,352.6	2	0.66	**5653.6**	1
23	20	5	*mem*	–	–	*mem*	–	–	1.56	36,000	1	0.89	**7125.5**	2
		10	*mem*	–	–	*mem*	–	–	4.64	36,000	1	0.74	**7852.6**	1
	40	5	*mem*	–	–	*mem*	–	–	2.25	36,000	2	0.64	**8142.8**	2
		10	*mem*	–	–	*mem*	–	–	5.32	36,000	2	0.94	**8754.2**	2
24	20	5	*mem*	–	–	*mem*	–	–	2.65	36,000	2	0.87	**9145.4**	1
		10	*mem*	–	–	*mem*	–	–	*mem*	–	–	0.78	**11,324.7**	1
	40	5	*mem*	–	–	*mem*	–	–	*mem*	–	–	**1.09**	36,000	2
		10	*mem*	–	–	*mem*	–	–	*mem*	–	–	**1.25**	36,000	1
Average			6.03[b]	24,882.9	1.0	3.70[b]	19,950.8	1.4	1.38[b]	13,238.3	1.4	0.68	**7070.8**	1.3

[a] Out of Memory.
[b] Instances where (a) did not contribute to the average calculation.

outperformed both algorithms [**PHA + HR + RH1**] and [**PHA + HR + RH2**] with respect to running time and solution quality. On average, algorithm [**PHA + HR + RH3**] provides a 18.3% and 29.1% faster solution than algorithms [**PHA + HR + RH1**] and [**PHA + HR + RH2**], respectively while dropping the average optimality gap from 1.52% and 1.77% to 0.84%. Overall, algorithm [**PHA + HR + RH3**] seems to offer high-quality solutions consistently within our experimental range.

The final set of experiments presents the results from solving model [**EVC**] using the algorithms proposed in Section 3 (shown in Table 6). To test the performance of the algorithms, we use *Case 19-24* from Table 3 (the largest test instances from Table 3) and vary sample size N and replication number M in the [**SAA**] algorithm to obtain 24 different problem instances. We set the large scenario $N' = 500$ to evaluate the [**SAA**] gap. We do not present the results obtained from CPLEX since CPLEX runs *out of memory* in solving all the problem instances reported in Table 6. Results indicate that [**SAA**] is able to solve only 4 out of 24 problem instances by obeying the pre-specified termination criteria. The performance improved slightly by incorporating Progressive Hedging Algorithm (PHA) inside the [**SAA**] framework, referred to as [**Hybrid-1**] algorithm. With this enhancement, [**SAA**] is now able to solve 8 out of 24 problem instances by obeying the pre-specified termination criteria. The benefits of using the algorithms become more pronounced when the heuristic enhancement strategies discussed under Section 3.3.1 and 3.3.2 are incorporated in the [**Hybrid-1**] algorithm, referred to as [**Hybrid-2**] algorithm. We observe that with these enhancement strategies, the average optimality gap of the [**Hybrid-2**] algorithm drops to 1.38% from 3.70% as reported in [**Hybrid-1**] algorithm. Further, the results in Table 6 indicate that the [**Hybrid-2**] algorithm is now capable of solving 16 out of 24 problem instances by obeying the pre-specified termination criteria. Finally, we observe a significant improvement in computational efficiency when the rolling horizon heuristic is incorporated in the [**Hybrid-2**] algorithm, referred to as [**Hybrid-3**] algorithm. Evidence from Table 4 and 5 shows that the rolling horizon heuristic variant [**RH3**] provides superior computational performance over the other two variants (*e. g.*, [**RH1**] and [**RH2**] algorithm). Thus, we utilize [**RH3**] algorithm inside the [**Hybrid-3**] algorithmic framework. With this enhancement, [**SAA**] is now able to solve 22 out of 24 problem instances by obeying the pre-specified termination criteria. We further observe that algorithm [**Hybrid-3**] on average saves 87.2% computation time over algorithm [**Hybrid-2**] in reporting the optimality gaps presented in Table 6. In summary, the [**Hybrid-3**] algorithm seems to offer consistently high-quality solutions within the experimental range.

5. Conclusion

This study develops an optimization framework that integrates both long-term planning decisions and short-term hourly operational decisions to design and manage electric vehicle charging station decisions over a pre-specified planning horizon and under power demand uncertainty. The proposed model **[EVC]** can be very challenging computationally depending on the size of the cells, years, hours, and scenarios set by the decision maker. To alleviate these challenges and to solve real scale problem instances, we develop a hybrid decomposition algorithm that combines Sample Average Approximation (SAA) with an enhanced Progressive Hedging Algorithm (PHA). The hybrid algorithm incorporates several algorithmic improvements such as penalty parameter updating techniques, local and global heuristics, and different variants of the rolling horizon heuristic. As evidenced from a set of computational results that the enhanced variant of the hybrid algorithm **[Hybrid-3]** is capable of producing high-quality solutions consistently to solve realistic large-size problem instances in a reasonable amount of time.

We use Washington, D.C. as a testing ground to evaluate the performance of the modeling results and to draw managerial insights. Our computational experiments reveal some insights about the impact of car charging percentage uncertainty on the design and management of charging stations. Further, we conduct sensitivity analysis on the impact of availabilities of grid power, solar power, and car discharging percentage for V2G power on system performance. It is observed that a 50% decrease in PG, solar power, and car discharging percentage for V2G power availability will open an additional 52.94%, 23.53%, and 14.70% charging stations in our tested region, respectively. Moreover, we observe that the system is highly sensitive to setting different minimum power demand requirements to open charging stations. Finally, we conduct sensitivity analysis with model **[EVE]** to see the impact of solar power utilization on system performance. Results indicate that the total system cost increases with an increase in solar utilization level but decreases with an increase in risk level. We believe that the models and results presented in this paper will help decision makers develop a future sustainable transportation system that will add value, not only to the economy, but also to the environment in which we live.

The major focus of our model is to cover both high- and low-level decisions for charging stations. We think that the main drive for the high-level decisions of locating charging stations is the performance of other already established stations. We see the inclusion of low-level decisions as a necessity to determine where to locate new stations, as the economic performance of already established facilities is a strong indication of whether there is a need to provide more. The majority of the parameters of the model are readily available for charging stations and can be easily obtained. Dividing the study area into cells and taking them all into consideration at once, as opposed to electing several locations, insures the elimination of potential error in assessing locations. We believe that it is more accurate, though exhausting and tiresome, to base the selection of the locations on performance and flow of electric vehicles at each and every segment of the grid, than to limit the choices. There might arise issues of the availability of land, but the cell selection should not be seen as rigid, but rather as an opportunity that can be seized in the surrounding region. Thus, this study will provide a more understandable and usable model for charging stations' investors to apply for future expansion.

This research also opens up a number of future research opportunities. The electric vehicles coming to a station, whether for charging or swapping, will have different levels of remaining power in their batteries. Thus, the unit power charging for each battery is considered to be variable. However, in this study we consider on average a constant unit power requirement for each car. Hence, one of the future research directions would be to incorporate the dynamicity of state-of-charge (SoC) to investigate its effect on the proposed two-stage stochastic problem. Our study also ignores the impact of traffic congestion in the designing and managing of electric vehicle charging stations. Furthermore, our study assumes that the network is robust and will never fail. However, in reality, electricity power can be disrupted due to natural (e.g., storms and severe weather, ice storms, hurricanes and tropical storms, tornadoes, and combination of extreme heat events and wildfires) or human-induced events (e.g., cyber attacks) which can severely impact the operational decisions of a charging station. These issues will be addressed in future studies.

Appendix A. Impact of solar power utilization on system performance

Renewable energy (*e. g*., solar and wind) curtailment occurs frequently to maintain system reliability, resulting in low utilization of these power resources. The main reason for renewable energy curtailment includes global oversupply, transmission or distribution congestion, and operational issues (Bird et al., 2014). The *National Renewable Energy Laboratory* (NREL) report, published in 2014, highlights the severity of renewable energy curtailment. For instance, in Texas, the average annual wind power curtailment was reported 16% of the total wind generation in 2009 (Rogers et al., 2010). The high solar and wind power curtailment has big impacts on the economics of the renewable power plant and will discourage investors, resulting a decrease in the usage of RES. Thus, the renewable resources operators are encouraged to utilize these powers to their largest possible extent. The chance-constrained stochastic optimization approach is used extensively in literature to ensure high renewable power utilization (Birge and Louveaux, 1997; Wang et al., 2012). However, the chance constraint ignores the scenario that occurs with lower probability but higher output. This eventually may lead to insufficient renewable power utilization. This low utilization of renewable power can be avoided if an expected value constraint is incorporated. Thus, we extend model [**EVC**] by introducing the following chance and expected value

Table 7
Systems performance under different solar power utilization and risk levels.

With different utilization levels			With different risk levels		
utilization χ (%)	Total cost ($)	CPU (sec)	Risk level ϵ (%)	Total cost ($)	CPU (sec)
50	18,223,017	3516	10	18,858,728	3385
60	18,476,658	3478	20	18,672,987	3425
70	18,672,404	3678	40	18,507,246	3486
80	18,859,358	3325	80	18,401,505	3504
90	18,929,212	3264	100	18,115,764	3574

constraints for each scenario $\omega \in \Omega$, referred to as [**EVE**].

$$\mathbb{P}\left\{\sum_{i\in\mathcal{I}}\sum_{h\in\mathcal{H}}(\lambda\eta_{ht\omega}f_{iht} - (G_{iht\omega} + Z_{iht\omega} + V_{iht\omega} + \right.$$
$$\left. \lambda B_{iht\omega})) \leqslant \Delta \quad \forall\ t \in \mathcal{T}\right\} \geqslant 1 - \epsilon \tag{71}$$

$$\mathbb{E}\left\{\sum_{i\in\mathcal{I}}\sum_{h\in\mathcal{H}} Z_{iht\omega}\right\} \geqslant \chi \mathbb{E}\left\{\sum_{i\in\mathcal{I}}\sum_{k\in\mathcal{K}}\sum_{h\in\mathcal{H}} r_{iht}^{\omega} Y_{ikt}\right\} \quad \forall\ t \in \mathcal{T} \tag{72}$$

Constraints (71) are joint chance-constraints which indicate that in each year $t \in \mathcal{T}$, there is at least $(1 - \epsilon)$ chance that the difference between the energy demand for electric vehicles ($\lambda\eta_{ht\omega}f_{iht}$) and the energy supply sources (e.g., grid, solar, V2G) lies below a threshold value Δ. Constraints (72) enforce that the utilization of solar energy resources should be greater than a certain percentage χ of the available solar energy $r_{iht\omega}$. Note that with this incorporation, the hybrid decomposition algorithm, proposed in Section 3, can no longer be applicable to solve model [**EVE**]. Therefore, we use the combined Sample Average Approximation (SAA) algorithm proposed by Zhao et al. (2014) to solve model [**EVE**]. We use Monte Carlo simulation to generate scenarios for renewable resources. We consider the historical data (Public Service Commission of the District of Columbia, 2016) of renewable resources in our tested region into account for predicting the future availabilities of solar power.

We now experiment with the impact of solar power utilization on system performance through solving model [**EVE**]. We define

(a) Year 2017   (b) Year 2018   (c) Year 2019

(d) Year 2020   (e) Year 2021
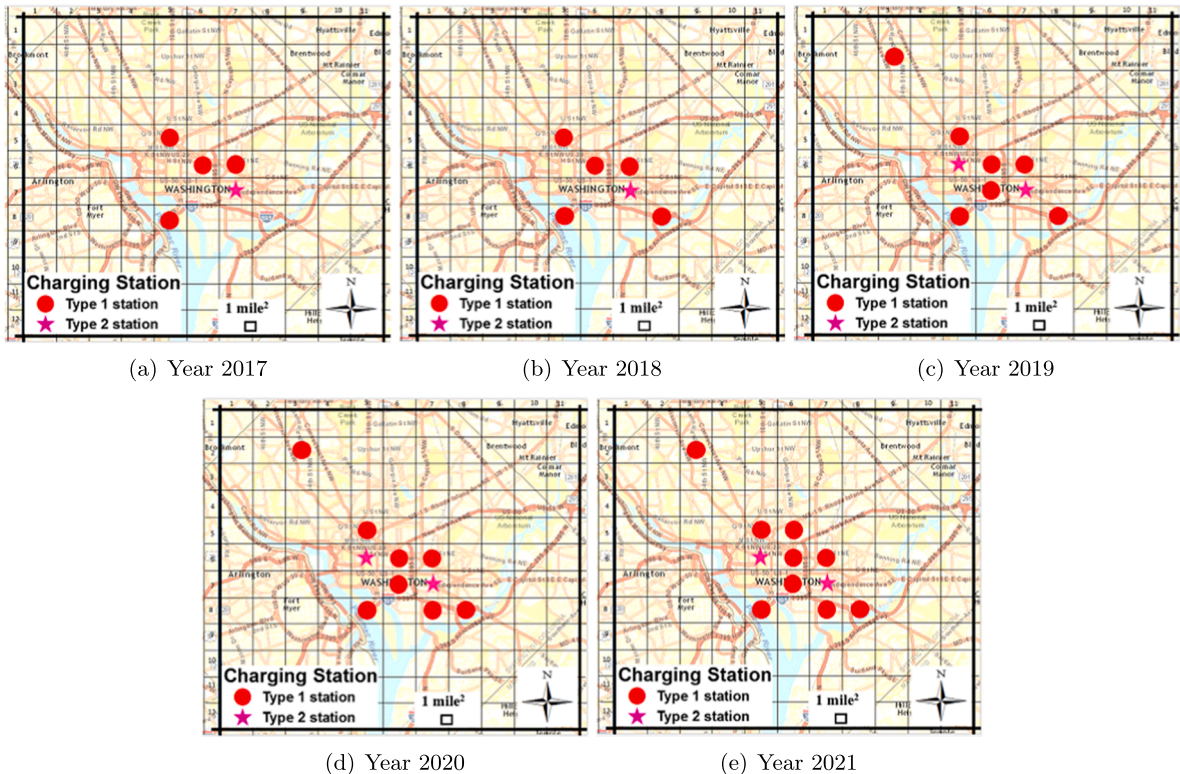
Fig. 15. Electric vehicle charging station location with expected value and chance constraint.

the small scenario set $N = 30$ and the large scenario $N' = 200$ to evaluate the SAA gap. The first set of experiments perform sensitivity analysis by setting different solar energy utilization levels χ to $\chi = \{50\%, 60\%, 70\%, 80\%, 90\%\}$ while fixing the risk level ϵ at 0.05. It is evident from the results in Table 7 that the total system cost increases as the solar utilization increases from 50% to 90%. This might be due to the incorporation of chance and expected value constraints (*i. e.*, constraints (71) and (72)), which enforce model [**EVE**] to become more restrictive, leading to an increase in total system cost. The second set of experiments perform sensitivity analysis on varying ϵ to $\epsilon = \{0.10, 0.20, 0.40, 0.80, 1.00\}$ while fixing the solar utilization χ to 80%. The results in Table 7 indicate that as the risk level ϵ increases from 10% to 100%, the total system cost reduces by 3.94% since constraints (71) become less restrictive as the risk level ϵ increases. A network representation for risk level $\epsilon = 0.10$ and solar utilization level $\chi = 80\%$ is depicted in Fig. 15. We observe that the scenario defined by incorporation of chance and expected value constraints (*i. e.*, constraints (71) and (72)) force model [**EVE**] to open more charging stations in a widespread distribution on our tested region compared to the base case results provided by model [**EVC**] in Fig. 6.

References

Agenbroad, J., Hollland, B., 2014. EV charging station infrastructure costs. Rocky Mountain Institute. Available from: <http://blog.rmi.org/blog_2014_04_29_pulling_back_the_veil_on_ev_charging_station_costs>.

ArcGIS, 2016. Washington, DC. Available from: <https://www.arcgis.com/home/item.html?id=009fd190135f40e1b4678b73a6ce7ef7>.

Bai, H., Miao, S., Zhang, P., Bai, Z., 2015. Reliability evaluation of a distribution network with microgrid based on a combined power generation system. Energies 8 (2), 1216–1241.

Balasubramanian, J., Grossmann, I., 2004. Approximation to multistage stochastic optimization in multiperiod batch plant scheduling under demand uncertainty. Indust. Eng. Chem. Res. 43 (14), 3695–3713.

Becker, T.A., Sidhu, I., Tenderich, B., 2009. Electric vehicles in the United States: a new model with forecasts to 2030. Center for Entrepreneurship and Technology, University of California, Berkeley, pp. 24.

Bento, N., 2008. Building and interconnecting hydrogen networks: insights from the electricity and gas experience in europe. Energy Policy 36 (8), 3019–3028.

Bhatti, S.F., Lim, M.K., Mak, H.Y., 2015. Alternative fuel station location model with demand learning. Ann. Oper. Res. 230 (1), 105–127.

Bird, L., Cochran, J., Wang, X., 2014. Wind and solar energy curtailment: experience and practices in the United States. US National Renewable Energy Laboratory (NREL).

Birge, J.R., Louveaux, F., 1997. Introduction to Stochastic Programming. New York, NY, USA.

Chen, B., Klampfl, E., Strumolo, M., Fu, Y., Chao, X., Tamor, M.A., 2017. Optimal investment strategies for light duty vehicle and electricity generation sectors in a carbon constrained world. Ann. Oper. Res. 255 (1–2), 391–420.

City Light, 2010. The Impact of Electric Vehicles on System Load. Available from: <https://www.seattle.gov/light/news/issues/irp/docs/dbg_538_app_d_3.pdf>.

Cornuejols, G., Nemhauser, G.L., Wolsey, L.A., 1983. The uncapacitated facility location problem (No. MSRR-493). Carnegie-mellon univ pittsburgh pa management sciences research group.

Crainic, T.G., Fu, X., Gendreau, M., Rei, W., Wallace, S.W., 2011. Progressive hedging-based metaheuristics for stochastic network design. Networks 58, 114–124.

Energy Information Administration, 2016. District of Columbia Profile State Profile and Energy Estimates. Available from: <http://www.eia.gov/state/?sid=DC#tabs-3>.

Fathabadi, H., 2015. Utilization of electric vehicles and renewable energy sources used as distributed generators for improving characteristics of electric power distribution systems. Energy 90, 1100–1110.

Ge, S., Feng, L., Liu, H., 2011. The planning of electric vehicle charging station based on grid partition method. In: 2011 International Conference on Electrical and Control Engineering, ICECE 2011 – Proceedings, pp. 2726–2730.

General Algebraic Modeling System (GAMS), 2013. Available from: <http://www.gams.com/>.

Gigaom, 2015. This is Tesla's first battery swap station. Available from: <http://gigaom.com/2015/01/29/this-is-teslas-first-battery-swap-station-photos/>.

Haddadian, G., Khalili, N., Khodayar, M., Shahidehpour, M., 2016. Optimal coordination of variable renewable resources and electric vehicles as distributed storage for energy sustainability. Sustain. Energy Grids Networks 6, 14–24.

He, Y., Venkatesh, B., Guan, L., 2012. Optimal scheduling for charging and discharging of electric vehicles. IEEE Trans. Smart Grid 3 (3), 1095–1105.

Hong, L., Pingliang, Z., Jianyi, G., Huiyu, W., Shaoyun, G., 2015. An optimization strategy of controlled electric vehicle charging considering demand side response and regional wind and photovoltaic. J. Modern Power Syst. Clean Energy 2 (2), 232–239.

Hosseini, M., MirHassani, S.A., 2015. Refueling-station location problem under uncertainty. Transp. Res. Part E: Logist. Transp. Rev. 84, 101–116.

Huang, Y., Fan, Y., Chen, C.-W., 2014. An integrated bio-fuel supply chain against feedstock seasonality and uncertainty. Transp. Sci. 48 (4), 540–554.

Hvattum, L.M., Lokketangen, A., 2009. Using scenario trees and progressive hedging for stochastic inventory routing problems. J. Heuristics 15, 527–557.

Ip, A., Fong, S., Liu, E., 2010. Optimization for allocating bev recharging stations in urban areas by using hierarchical clustering. In: 2010 6th International Conference on Advanced Information Management and Service (IMS), pp. 460–465.

Jin, C., Sheng, X., Ghosh, P., 2014. Optimized electric vehicle charging with intermittent renewable energy sources. IEEE J. Sel. Top. Signal Process. 8 (6), 1063–1072.

Kavousi-Fard, A., Khodaei, A., 2016. Efficient integration of plug-in electric vehicles via reconfigurable microgrids. Energy 111, 653–663.

Kleywegt, A.J., Shapiro, A., Homem-De-Mello, T., 2001. The sample average approximation method for stochastic discrete optimization. SIAM J. Optim. 12, 479–502.

Kuby, M., Lim, S., 2005. The flow-refueling location problem for alternative-fuel vehicles. Soc.-Econ. Plann. Sci. 39 (2), 125–145.

Li, S., Huang, Y., Mason, S.J., 2016. A multi-period optimization model for the deployment of public electric vehicle charging stations on network. Transp. Res. Part C: Emerg. Technol. 65, 128–143.

Liu, C., Wang, J., Botterud, A., Zhou, Y., Vyas, A., 2012. Assessment of impacts of PHEV charging patterns on wind-thermal scheduling by stochastic unit commitment. IEEE Trans. Smart Grid 3 (2), 675–683.

Liu, N., Chen, Z., Liu, J., Tang, X., Xiao, X., Zhang, J., 2014. Multi-objective optimization for component capacity of the photovoltaic-based battery switch stations: towards benefits of economy and environment. Energy 64, 779–792.

Liu, W., Niu, S., Xu, H., Li, X., 2016. A new method to plan the capacity and location of battery swapping station for electric vehicle considering demand side management. Sustainability 8 (6), 557.

Mak, H.Y., Rong, Y., Shen, Z.M., 2013. Infrastructure planning for electric vehicles with battery swapping. Manage. Sci. 59 (7), 1557–1575.

Marino, C., Quddus, M.A., Marufuzzaman, M., Cowan, M., Bednar, A.E., 2018. A chance-constrained two-stage stochastic programming model for reliable microgrid operations under power demand uncertainty. Sustainable Energy, Grids Networks 13, 66–77.

Nilsson, M., 2011. Electric vehicles: The phenomenon of range anxiety. ELVIRE, Gif-sur-Yvette Cedex, France, ELVIRE Consortium FP7CICT-2009C4-249105.

Nurre, S.G., Bent, R., Pan, F., Sharkey, T.C., 2014. Managing operations of plug-in hybrid electric vehicle (PHEV) exchange stations for use with a smart grid. Energy Policy 67, 364–377.

Ortega-Vazquez, M.A., Bouffard, F., Silva, V., 2013. Electric vehicle aggregator system operator coordination for charging scheduling and services procurement. IEEE Trans. Power Syst. 28 (2), 1806–1815.

Pan, F., Bent, R., Berscheid, A., Izraelevitz, D., 2010. Locating phev exchange stations in v2g. In: 2010 First IEEE International Conference on Smart Grid

Communications, pp. 173–178.

Plug in America, 2016. EV Battery Amortization Costs and Vehicle To Grid. Available from: <http://pluginamerica.org/ev-battery-amortization-costs-and-vehicle-grid/>.

Plug In Sites, 2014. News about electric car charging stations in DC, Maryland, Virginia & beyond. Available from: <http://pluginsites.org/how-many-plug-in-electric-vehicles-are-in-md-va-dc/>.

Poudel, S., Marufuzzaman, M., Quddus, M.A., Chowdhury, S., Bian, L., Smith, B., 2018. Designing a reliable and congested multi-modal facility location problem for biofuel supply chain network. Energies 11 (7), 1682.

Poudel, S.R., Quddus, M.A., Marufuzzaman, M., Bian, L., Burch, R., 2017. Managing congestion in a multi-modal transportation network under biomass supply uncertainty. Ann. Oper. Res. 1–43.

Public Service Commission of the District of Columbia, 2016. Report on the Renewable Energy Portfolio Standard for Compliance Year 2015. Available from: <http://www.dcpsc.org/getmedia/901b3c18-4859-435d-ae1a-ca296584c26b/aharris_542016_831_1_FC_-_945_-_2016_-_E_-_REPORT.aspx>.

Quddus, M., 2018. Models and Algorithms to Solve Electric Vehicle Charging Stations Designing and Managing Problem Under Uncertainty. Mississippi State University.

Quddus, M.A., Chowdhury, S., Marufuzzaman, M., Yu, F., Bian, L., 2018. A two-stage chance-constrained stochastic programming model for a bio-fuel supply chain network. Int. J. Prod. Econ. 195, 27–44.

Quddus, M.A., Shahvari, O., Marufuzzaman, M., Usher, J.M., Jaradat, R., 2018. A collaborative energy sharing optimization model among electric vehicle charging stations, commercial buildings, and power grid. Appl. Energy 229, 841–857.

Quddus, M.A., Yavuz, M., Usher, J.M., Marufuzzaman, M., 2019. Managing load congestion in electric vehicle charging stations under power demand uncertainty. Expert Syst. Appl. 125, 195–220.

Rockafellar, R.T., Wets, R.J.-B., 1991. Scenarios and policy aggregation in optimization under uncertainty. Math. Oper. Res. 16, 119–147.

Rogers, J., Fink, S., Porter, K., 2010. Examples of Wind Energy Curtailment Practices. Subcontract Report NREL.

Salt River Project, 2015. Electric Vehicle Price Plan. Available from: <http://www.srpnet.com/prices/home/electricvehicle.aspx>.

Shojaabadi, S., Abapour, M., Nahavandi, A., 2016. Optimal planning of plug-in hybrid electric vehicle charging station in distribution network considering demand response programs and uncertainties. IET Gener. Transm. Distrib. 10 (13), 3330–3340.

Solar Cell Central, 2016. Solar Electricity Costs. Available from: <http://solarcellcentral.com/cost_page.html>.

Sweda, T., Klabjan, D., 2011. An agent-based decision support system for electric vehicle charging infrastructure deployment. In: Vehicle Power and Propulsion Conference (VPPC), 2011 IEEE. pp. 1–5.

Trochaniak, S., 2016. Electric Vehicle Sales in the United States: 2016 Final Update. Available from: <http://www.fleetcarma.com/ev-sales-usa-2016-final/>.

U.S. Department of Energy, 2014. EV Everywhere Grand Challenge Road to Success. Available from: <http://energy.gov/sites/prod/files/2014/02/f8/eveverywhere_road_to_success.pdf>.

Vries, H.D., Duijzer, E., 2017. Incorporating driving range variability in network design for refueling facilities. Omega 69, 102–114.

Wang, H., Huang, Q., Zhang, C., Xia, A., 2010. A novel approach for the layout of electric vehicle charging station. In: 2010 International Conference on Apperceiving Computing and Intelligence Analysis, ICACIA 2010 – Proceeding, pp. 64–70.

Wang, Q., Guan, Y., Wang, J., 2012. A chance-constrained two-stage stochastic program for unit commitment with uncertain wind power output. IEEE Trans. Power Syst. 27 (1), 206–215.

Washington State Department of Transportation, 2015Washington State Electric Vehicle Action Plan. Available from: <http://www.wsdot.wa.gov/NR/rdonlyres/28559EF4-CD9D-4CFA-9886-105A30FD58C4/0/WAEVActionPlan2014.pdf>.

Weiller, C., Sioshansi, R., 2016. The role of plug-in electric vehicles with renewable resources in electricity systems. Available from: <http://ise.osu.edu/isefaculty/sioshansi/papers/pev_renewables.pdf>.

Worley, O., Klabjan, D., 2011. Optimization of battery charging and purchasing at electric vehicle battery swap stations. In: 2011 IEEE Vehicle Power and Propulsion Conference, pp. 1–4.

Zhao, C., Wang, Q., Wang, J., Guan, Y., 2014. Expected value and chance constrained stochastic unit commitment ensuring wind power utilization. IEEE Trans. Power Syst. 29 (6), 2696–2705.